

Dear Editor and Reviewers:

Thank you for your letter and for reviewers' valuable comments and questions concerning our manuscript entitled "Error analyses of a multistatic meteor radar system to obtain a 3-dimensional spatial resolution distribution" [MS no. amt-2020-353]. We have studied the valuable comments from you and reviewers carefully, and tried our best to revise the manuscript. I sincerely apologize for my poor English writing that have made revised manuscript hard to read. Therefore, Prof. Reid and other coauthor had polished manuscript again. We hope that you could be satisfied with the new revision. These changes in the revise manuscript have been marked blue in the track changes version manuscript, as well as the point to point responses have listed as following:

Response to reviewer #1:

General comments:

- 1) Only the issue of mutual antenna coupling was not picked up in detail.

Response: We are sorry for our insufficient discussion about mutual antenna coupling. We only limit the elevation angle to avoid the effect of mutual antenna coupling, although HFSS can evaluate this effect. We mainly discuss the error propagation in general situation and due to space limitations, we only simply mention this effect. However, in the future work that discuss a specific radar system, we will discuss some issues suggested by you including mutual antenna coupling in detail. For example, we intend to do some work about meteor radar detection in low altitude and low elevation angle, thus HFSS is a powerful tool for our study. Thanks for your suggestion about HFSS very much.

Minor suggestions/technical corrections:

- 1) Vertical wind (line 33-34):

This statement is not true. There are publications that do not use this assumption, but there is no validation available whether these winds are scientifically useful (see Egito et al., 2016, Stober et al., 2020, Stober et al., 2021, Conte et al., 2021, Chau et al., 2020, etc). Considering the huge systematic issues in stated values, it is recommended to weaken a bit the statement. But vertical winds provide a very good quality assessment of the retrieval and, thus are important.

Response: Very kind of you for your comments and suggestion. Following your suggestion, we add "usually" in front of "a zero wind " to weaken a bit statement.

2) MIMO, SIMO, etc (line 53-55):

The first statistical MIMO radar was not Chau et al., 2019 a better citation is the French RIAS system. It operated in the meteor wavelength range and consisted of two circular arrays. However, the focus was not directly on atmospheric dynamics, but the concept is rather old. Please add the citation. J. Dorey, Y. Blanchard, F. Christophe, “Le projet RIAS, une approche nouvelle du radar de surveillance aérienne”, Colloque International sur le radar, 1984, Versailles, France.

Response: Thanks for your comments very much. We add this reference in new version.

3) Discussion of measurement response (line 295-310):

The reviewer provided a statement in his review about the measurement response. The reply of the authors and revising in the manuscript is appreciated. The reviewer apologizes for being not specific enough on that topic. The paragraph requires no changes, although the term measurement response is not used in its mathematical context. The measurement response describes how much an observation reduces an a priori covariance for a certain state. The measurement response provides a mathematical assessment of the observations, the forward model, and all error contributions intrinsic to the observations. However, this goes beyond the paper.

Response: Thanks for your comments very much. The issues about measurement response and the priori covariance et.al. will be emphatically discussed in our future work. These issues are important for wind retrieving. In line 353-365 in tracked changes version, we reorganized the language to make it more accurate.

4) Conclusion (line 324) :

The statement about SIMO is questionable as the paper does not investigate any advantages or disadvantages between the systems. So please remove the statement advantage. Time will tell which system advantageous.

Response: Thanks for your comments very much. We apologize for our unreasonable statement. Following your suggestion, we change the sentence in line 381-382 to “also show good experimental results ~~and have some advantages over SIMO systems~~”

Response to reviewer #2:

1) In the first place, I am wondering if the size of the sampling grid used to do the error analysis is the proper one. 5 x 5 km in the horizontal plane seems a bit small to have good statistics in order to obtain reliable estimates of the location errors (lines 298-301 in the tracked changes file).

Response: Thanks for your comments very much. The selection of a suitable “horizontal sampling measurement area” for multistatic meteor radars is a good question. As Figure 8 shows, a meteor event’s horizontal location error can exceed

15km or more in some effective measuring region. Therefore, take (Stober, et.al. 2018) for example, the sampling area in horizontal is 30 x 30km. However, the “horizontal sampling grid length” in our manuscript is a default calculation length in program. This sampling grid length can be set to larger value to reduce computational cost or smaller to make contourf more elaborate. But the calculation results, that’s to say, spatial resolutions, will determine the values of suitable “horizontal sampling measurement area”. In the region where horizontal resolution is low, “horizontal sampling measurement area” will chose to be larger. While in high resolution region, “horizontal sampling measurement area” could chose to be smaller. The issues of selecting a suitable “horizontal sampling measurement area” will be discussed in future work.

- 2) Second, the English writing is still not good for a prestigious journal like AMT. I mean this with all due respect, but it happened many times that I thought I was reading a telegram. There is no coherence among many sentences. Punctuation marks are missing or sometimes they are not used properly. Countless “the” articles are missing. At one point, I just stopped correcting all these mistakes, so I will only provide some examples.

Response: Thanks for your suggestions very much. The revised manuscript is changed a lot comparing with original one and didn’t polished well for time’s sake. Thereby, I sincerely apologize for my poor English writing that have made revised manuscript hard to read. Prof. Reid and other coauthor had helped me polished manuscript again. We hope that you could be satisfied with the new revision.

The following examples apply to the line numbering that corresponds to the tracked changes file.

- 1) Line 29: change to “... detected by meteor radars, regardless of the weather conditions”.
corrected
- 2) Line 31: change to “Most modern meteor radars are monostatic.”
corrected
- 3) Line 39: “~~look~~ viewing direction”
corrected
- 4) Lines 53: instead of “and measurements of the non-homogenous wind fields”, I suggest to write something like “and sampling the observed area from different viewing angles”.
Corrected. Thanks for your suggestion.
- 5) Line 59: it is better to say that multistatic meteor radars have “several” or “a few” advantages over monostatic ones, rather than “many”.
Corrected. Thanks for your suggestion.
- 6) Lines 67-68: what do the authors mean with “are described in the references in these papers”?

We apologize for our language errors that mislead you. In line 67-68 in tracked changes version, we correct it to “are described in the corresponding references.”

- 7) Line 69: I think the authors wanted to say “areas of interest” and not “interested areas”.

Yes. Corrected.

- 8) Line 89: “... influence on spatial resolution distribution due to ignore the discussion of radial distance measuring error” - I think the authors mean something like “... influence on the spatial resolution distribution because it ignores the discussion of radial distance measuring error.”

Yes. Corrected.

- 9) Line 105: “... one is those that caused by the zenith angle measuring error...” This does not make sense. Line 106: “... and another is those that caused by the pulse length effect...” Again, this is incorrect English writing.

Thanks for you comments. In new version, we corrected it to “one caused by..., and one caused...”

- 10) Line 108: “... passes through...”

Corrected.

- 11) Line 112: “... meteor event meanwhile...” should be changed to “... meteor event, meaning...”

Corrected.

- 12) Line 118: “in plan view”?

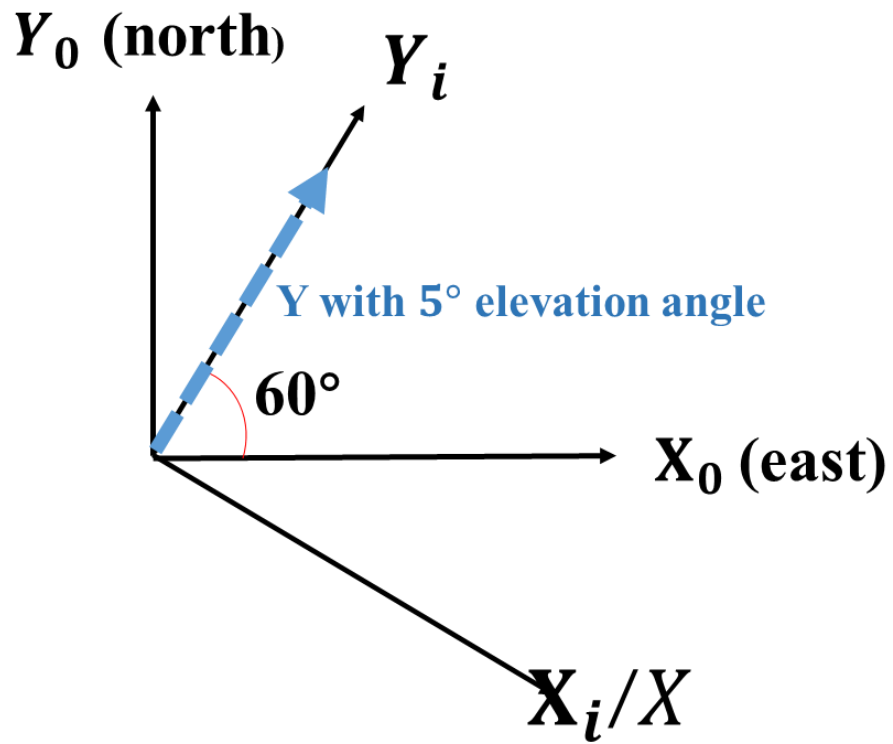
Means “”, maybe better

- 13) Line 165: “... by rotating clockwise in order of ...” Did the authors mean “rotating orderly”?

Yes, Corrected.

- 14) Line 290: What does “... points to east by north 60°” really mean? And why 60°?

Thanks for you comments. In manuscript we take “ $\psi_x^{i,0} = \psi_y^{i,0} = 0$, $\psi_z^{i,0} = 30^\circ$ and $d_i = 250km$; $\psi_x^{X,i} = 5^\circ, \psi_y^{Y,i} = 0, \psi_z^{Z,i} = 0$ ” for example. “ $\psi_x^{i,0} = \psi_y^{i,0} = 0$, $\psi_z^{i,0} = 30^\circ$ ” means that axis- X_i points to 30° east by south thus axis- Y_i points to east by north 60° . “ $\psi_x^{X,i} = 5^\circ, \psi_y^{Y,i} = 0, \psi_z^{Z,i} = 0$ ” means that axis-X is collinear with axis- X_i and axis-Y has 5° elevation angle right above axis- Y_i . See image below.



15) Line 300: change to "... with equal probability..."

Corrected.

Error analyses of a multistatic meteor radar system to obtain a 3-dimensional spatial resolution distribution

Wei Zhong^{1,2}, Xianghui Xue^{1,2,3}, Wen Yi^{1,2}, Iain M. Reid^{4,5}, Tingdi Chen^{1,2,3}, Xiankang Dou^{1,6}

¹CAS Key Laboratory of Geospace Environment, Department of Geophysics and Planetary Sciences, University of Science and Technology of China, Hefei, China

²Mengcheng National Geophysical Observatory, School of Earth and Space Sciences, University of Science and Technology of China, Hefei, China

³CAS Center for Excellence in Comparative Planetology, Hefei, China

⁴ATRAD Pty Ltd., Thebarton, South Australia, Australia

⁵School of Physical Sciences, University of Adelaide, Adelaide, South Australia, Australia

⁶Wuhan University, Wuhan, China

Correspondence to: Xianghui Xue (xuexh@ustc.edu.cn)

Abstract: In recent years, the concept of multistatic meteor radar systems has attracted the attention of the atmospheric radar community, focusing on the mesosphere and lower thermosphere (MLT) region. Recently, there have been some notable experiments using such multistatic meteor radar systems. Good spatial resolution is vital for meteor radars because nearly all parameter inversion processes rely on the accurate location of the meteor trail specular point. It is timely then for a careful discussion focussed on the error distribution of multistatic meteor radar systems. In this study, we discuss the measurement errors that affect the spatial resolution and obtain the spatial resolution distribution in 3-dimensional space for the first time. The spatial resolution distribution can both help design a multistatic meteor radar system and improve the performance of existing radar systems. Moreover, the spatial resolution distribution allows the accuracy of retrieved parameters such as the wind fields to be determined.

1 Introduction

The mesosphere and lower thermosphere (MLT) is a transition region from the neutral to the partially ionized atmosphere. It is dominated by the effects of atmospheric waves, including planetary waves, tides and gravity waves. It is also a relatively poorly sampled part of the Earth's atmosphere by ground-based instruments. One widely used approach to sample this region is the meteor radar technique. The ablation of incoming meteors in the MLT region, i.e., ~80 – 110 km, creates layers of metal atoms, which can be observed from the ground by photometry or lidar (Jia et al., 2016; Xue et al., 2013). During meteor ablation, the trails caused by small meteor particles provide a strong atmospheric tracer within the MLT region that can be continuously detected by meteor radars, regardless of weather conditions. Consequently, the meteor radar technique has been a powerful tool for studying the MLT region for decades (Hocking et al., 2001; Holdsworth et al., 2004; Jacobi et al., 2008; Stober et al., 2013; Yi et al., 2018). Most modern meteor radars are monostatic, and this has two main limitations in

retrieving the complete wind fields. Firstly, limited meteor rates and relatively low measurement accuracies necessitate that all measurements in the same height range are processed to calculate a “mean” wind. Secondly, classic monostatic radars retrieve ~~windwinds~~ based on the assumption of a homogenous wind in the horizontal and usually a zero wind in the vertical direction.

The latter conditions can be partly relaxed if the count rates are high and the detections are distributed through a representative range of azimuths. If this is the case, a version of a Velocity Azimuth Display (VAD) analysis can be applied by expanding the zonal and meridional winds using a truncated Taylor expansion (Browning and Wexler, 1968). This is because each valid meteor detection yields a radial velocity in a particular ~~lookviewing~~ direction of the radar. The radar is effectively a multi-
40 beam Doppler radar where the “beams” are determined by the meteor detections. If there are enough suitably distributed detections in azimuth in a given observing period, the Taylor expansion approach using cartesian coordinates yields the mean zonal and meridional wind components (u_0, v_0) , the horizontal divergence $\left(\frac{\partial u}{\partial x} + \frac{\partial v}{\partial y}\right)$, the stretching $\left(\frac{\partial u}{\partial x} - \frac{\partial v}{\partial y}\right)$ and the shearing $\left(\frac{\partial u}{\partial y} + \frac{\partial v}{\partial x}\right)$ deformations of the wind fields from an analysis of the radial velocities. However, because the radar can only retrieve the wind projection in the radial direction as measured from the radar, the vorticity $\left(\frac{\partial v}{\partial x} - \frac{\partial u}{\partial y}\right)$ of the wind fields
45 is not available. This is common to all monostatic radar systems and a discussion of measurable parameters in the context of multiple fixed beam upper atmosphere Doppler radars is given by (Reid, 1987). Even by relaxing the assumption of a homogeneous wind fields and using the more advanced Volume Velocity Processing (VVP) (Philippe and Corbin, 1979) to retrieve the wind fields, the horizontal gradients of the wind fields cannot be recovered due to the lack of vorticity information. To obtain a better understanding of the spatial variation of the MLT region wind fields, larger area observations (and hence
50 higher meteor count rates) and ~~measurements of sampling the non homogenous wind fields~~ observed area from different viewing angles are needed. An extension of the classic monostatic meteor technique is required to satisfy these needs.

To resolve the limitations outlined above, the concept of multistatic meteor radar systems, such as MMARIA (multi-static and multi-frequency agile radar for investigations of the atmosphere) (Stober and Chau, 2015) and SIMO (single input multiple output) (Spargo et al., 2019), MIMO (multiple input multiple output radar) (Chau et al., 2019; DOREY et al., 1984) have been
55 designed and implemented (Stober et al., 2018). Multistatic systems can utilize the forward scatter of meteor trails, thus providing another perspective for observing the MLT. Multistatic meteor radar systems have ~~manyseveral~~ advantages over classic monostatic meteor radars, such as obtaining higher-order wind ~~fieldsfield~~ information and covering wider observation areas. There have been some particularly innovative studies using multistatic meteor radar systems in recent years. For example, by combining MMARIA and the continuous wave multistatic radar technique (Vierinen et al., 2016), Stober ~~and Chau et al.~~
60 ~~built a 5 station total 7 link multistatic radar network covering an approximately 600 km×600 km region in Germany to retrieve an arbitrary non homogenous wind fields with a 30 km×30 km horizontal resolution (Stober et al., 2018). Chau et al.~~ et al. (2018) built a 5-station 7-link multistatic radar network covering an approximately 600 km×600 km observing region over Germany to retrieve an arbitrary non-homogenous wind field with a 30 km×30 km horizontal resolution. Chau et al.

(2017) used two adjacent classic monostatic specular meteor radars in northern Norway to obtain horizontal divergence and vorticity (Chau et al., 2017). Other approaches, such as coded continuous wave meteor radar (Vierinen et al., 2019) and the compressed sense method in MIMO sparse signal recovery (Urco et al., 2019), are described in the corresponding references in these papers.

Analysing spatial resolution in interested areas limits is a fundamental but difficult topic for meteor radar systems. Meteor radar systems transmit radio waves and then receive radio waves reflected from meteor trails using a cluster of receiver receiving antennas; commonly five antennas as in the Jones et al. (1998) configuration (Jones et al., 1998). By analysing the cross correlation correlations of the signals received signals, one can determine on several pairs of antennas, the angle of arrivals (AoAs) which includes arrival (AoA) of each return can be determined. The AoA is described by the zenith angle θ and azimuth angle denoted as θ and ϕ respectively. By measuring the wave propagation time, one can obtain from the meteor trail, range information can be determined. Most meteor radar systems rely on specular reflections from meteor trails. Thus, by combining the AoAs/AoA and the range information and then using geometric analysis, one can determine the location of a meteor trail/trail can be determined. Accurately locating the meteor trail specular point (MTSP hereafter/hereinafter) is important since atmospheric parameter retrieval (such as the wind fields/field or the temperature) depends on the location information of meteor trails. The location accuracy, namely the spatial resolution, determines the reliability of the retrieved parameters. For multistatic meteor radar systems that/which can relax the assumption of a homogenous horizontal wind fields/field, the location accuracy becomes a more important issue because the horizontal spatial resolution affects the accuracy of the retrieved horizontal wind fields/gradient/field.

There are some discussions about measuring Although meteor radar systems have developed well experimentally in recent years, the reliability of the retrieved atmospheric parameters still requires further investigation for both the monostatic and multistatic meteor radar cases. In an attempt to investigate errors of the meteor radar. For example, a in two radar techniques, Wilhelm et al. (2017) compared 11 years of MLT region wind data from a partial reflection (PR) radar with collocated monostatic meteor radar winds and determined the ‘correction factors’ to bring the winds into agreement. Reid et al. (2018) reported a similar study for two locations for data obtained over several years. While the comparisons are interesting, partial reflection radars operating in the medium frequency (MF) and lower high frequency (HF) bands produce a height dependent bias in the measured winds (see e.g., Reid, 2015) which limits the ability to estimate errors in the meteor winds by comparing with them. However, the PR radar technique is one of very few that provides day and night coverage and data rates in the MLT comparable to that of meteor radars.

Meteor radars have largely replaced PR radars for MLT studies and are generally regarded as providing reference quality winds. It is essential then to know the reliability of atmospheric parameters determined by meteor radars and to do this, some quantitative error analyses are necessary.

A number of recent studies have discussed AoAs measuring/AoA measurement errors for meteor radars (Kang, 2008; Vaudrin et al., 2018; Younger and Reid, 2017). However, these/These studies focus on the phase errors in receiver antennas/antenna pairs; Younger and seldom discuss/Reid for the influence of monostatic case, and Vaudrin et al. for a more general case which

~~included multistatic configuration on the spatial resolutions~~ meteor radars. Hocking (2018) used another approach and developed a vertical resolution analysis method ~~in a for the~~ 2-dimensional ~~baseline vertical section~~ (Hocking, 2018), which ~~bistatic case.~~ Hocking's method (HM hereinafter) simplifies the error propagation process in ~~receiver~~the receiving antennas and ~~puts~~ emphasis on how a bistatic meteor radar configuration ~~would affect~~affects the vertical resolution in a vertical section. ~~However, Hocking's method (HM hereinafter) can barely show bistatic configurations' influence on spatial resolution distribution due to ignore the discussion of~~It does not consider the radial distance measuring error. ~~Moreover, HM is only a demo about vertical resolution in a specific vertical section, not in real three-dimensional space. Hence, for practical purposes,~~ ~~the~~In this paper, we consider the more general 3-dimensional ~~case and determine the~~ spatial distribution of both ~~the~~ horizontal resolution and vertical resolution ~~should be considered~~uncertainties.

~~Although multistatic meteor radar systems have developed well experimentally in recent years, the reliability of retrieved atmospheric parameters lacks discussion both for monostatic and multistatic meteor radar. A large part of the reason is that no other measurement technology can provide contrast data for meteor radars in MLT region. On the one hand it proves that meteor radars are irreplaceable in MLT region as a measurement technology; on the other hand, to know the reliability of meteor radars obtained atmospheric parameters and to get better understanding of the dynamic process in MLT region, some quantitative error analyses are necessary and helpful. In this paper, we~~We analyse the multistatic meteor radar resolution distribution in a three-dimensional space for both vertical and horizontal resolution for the first time. ~~And~~This spatial resolution is a prerequisite for evaluating the reliability of retrieved atmospheric parameters, such as ~~the~~ wind ~~fields~~field and ~~the~~ temperature.

2 Analytical Method

2.1 ~~brief~~Brief introduction

The HM will be introduced ~~ahead in short~~briefly here to help understand our ~~method~~generalization. In the HM, ~~measuring~~measurement errors that affect ~~the~~ vertical resolution can be classified into two types (~~Hocking, 2018~~): one ~~is those~~ that caused by the zenith angle measuring error $\delta\theta$ and ~~another is those that~~one caused by the pulse-length effect on ~~the~~ vertical resolution. The ~~receiver~~receiving array is a simple antenna pair that is collinear ~~to~~with the baseline (figure 1). ~~The~~ HM ~~only calculate~~calculates the vertical resolution in a two-dimensional vertical section which ~~pass through~~passes through the baseline. The receiver antenna pair is equivalent to one receiver arm in a Jones configuration which is comprised of three collinear antennas ~~and is~~ usually in a $2\lambda \setminus 2.5\lambda$ ~~configuration.~~ Phasespacing. The phase difference of ~~the~~ received radio wave between ~~the~~ receiving antenna ~~pairs~~pair is denoted as $\Delta\Psi$. In meteor radar systems, there ~~are~~is generally an 'acceptable' phase difference measuring error (PDME ~~hereafter~~hereinafter) $\delta(\Delta\Psi)$. A higher value of $\delta(\Delta\Psi)$ means that more detected signals will be judged as a meteor ~~event~~ meanwhile events, but with more misidentifications and bigger errors as well. $\delta(\Delta\Psi)$ is set to approximately 30° (Hocking, 2018; Younger and Reid, 2017) in ~~most~~ meteor radar systems. In the HM, the zenith angle

measuring error $\delta\theta$ is due to $\delta(\Delta\Psi)$ and $\delta(\Delta\Psi)$ is a constant. Therefore, the error propagation in the receiver is very simple,
130 and $\delta\theta$ is inversely proportional to the cosine of the zenith angle.

~~Now~~We now introduce our analytical method. Our method considers a multistatic system with multiple transmitters and one
receiverreceiving array in 3-dimensional space (as shown in figure 2). The receiverreceiving array is in the Jones configuration,
which can be that is, “cross-shaped”, “but it may also be “T-shaped” or “L-shaped” in plan view. The five receiver antennas
are in the same horizontal plane and constitute two orthogonal antenna arms. To avoid a complex error propagation process in
135 receiverthe receiving array and to place emphasis on multistatic configurations, the PDMs in the two orthogonal antenna
arms ($\delta(\Delta\Psi_1)$ and $\delta(\Delta\Psi_2)$) are constants. Therefore, the AoAsAoA measuring errors (including the zenith and azimuth angle
measuring errors $\delta\theta$, $\delta\phi$ respectively) can be expressed as a simple functionfunctions of zenith and azimuth angle. The radial
distance is the distance between the MTSP and the receiver, which is denoted as R_s . R_s can be determined by combining the
AoAsAoA, baseline length d_i , and the radio wave propagatingpropagation path length R (Stober and Chau, 2015). SeeThe
140 geometry is shown in figure 4(a). α is the angle between the baseline (i.e., axis- X_i) and the line from the receiver to the
MTSP, if(denoted as point A). If α , d_i and R are known, R_s willcan be calculated easily using the Cosine Law as:

$$R_s = \frac{R^2 - d_i^2}{2(R - d_i \cos\alpha)} \quad (1)$$

~~α is the angle between the baseline (i.e., axis- X_i) and the line from the receiver to the MTSP denoted as point A. The~~
multistatic configuration will influence the accuracy of R_s (denoted as δR_s). This is because ~~that~~ α , d and R are determined
145 by the multistatic configuration. We consider the error term δR_s in our method, which is ignored in the HM. δR_s is a function
of the AoAsAoA measuring errors ($\delta\theta$ and $\delta\phi$) and the radio wave propagation path length measuring error (denoted as δR).
 δR is caused by the measuring error of the wave propagation time δt , which is approximately $21\mu s$ (Kang, 2008). Thus, δR
can be set as a constant and the default value in our program is $\delta R = c\delta t = 6.3km$. It is worth noting that the maximum
unambiguous range for pulse meteor radars is determined by the pulse repetition frequency (PRF) (Hocking et al., 2001;
150 Holdsworth et al., 2004). For multistatic meteor radars utilizing forward scatter, the maximum unambiguous range is c/PRF
(where c is the speed of light). For the area where R exceedexceeds the maximum unambiguous range, δR is set to positive
infinity.

2.2 ~~three~~Three kinds of coordinate systems and their transformations

To better depict the multistatic system configuration, three kinds of right-hand coordinate systems (figure-3) need to be
155 established, which as shown in figure 3. These are $X_0Y_0Z_0$, $X_iY_iZ_i$ and XYZ. $X_0Y_0Z_0$ is the ENU (east-north-up) coordinate
system andwhere axis- X_0, Y_0, Z_0 represent the east, north, up directions respectively. Another two coordinate systems are
established to facilitate different error propagations. All types of errors need to be transformed to the ENU coordinate system
 $X_0Y_0Z_0$ in the end. Coordinate system XYZ is established to depict the spatial configuration of the receiver. XYZ is fixed on

receiving array and has its the receiver. See figure 3, the coordinate origin of XYZ is on the receiver there as shown in figure
 160 3. Axis-Z is collinear with the antenna boresight and perpendicular to the receiver-horizontal plane on which the receiving
 array lies. Axis-X and axis-Y are collinear with the arms of the two orthogonal antenna arrays. AoAs will be represented
 in XYZ for convenience. See Inspection of figure 4, indicates that it is convenient to analyse the range information in a plane
 that goes through the baseline and the MTSP. Thus, a coordinate system $X_i Y_i Z_i$ is established for a transmitter T_i . The
 coordinate origins of $X_i Y_i Z_i$ are all on the receiver-receiving array. We stipulate that axis- X_i points to transmitter i (T_i). Each
 165 pair of T_i and the receiver R_x constitute/constitutes a radar link, which is referred to as L_i . The range related information for
 each L_i will be calculated in $X_i Y_i Z_i$. Different types of errors need to propagate to and be compared in $X_0 Y_0 Z_0$ which is
 convenient for retrieving wind fields.

We stipulate that clockwise rotation satisfies the right-hand corkscrew rule. By rotating ~~clockwise in order of~~ $\psi_x^{X,i}$, $\psi_y^{Y,i}$ and
 $\psi_z^{Z,i}$ about axis- X , Y and Z , respectively, one can transform XYZ to $X_i Y_i Z_i$. It is worth mentioning that $X_i Y_i Z_i$ is non-unique
 170 because any rotation about axis- X_i can obtain another satisfactory $X_i Y_i Z_i$. Hence, $\psi_x^{X,i}$ can be set to any values/value. Similarly,
 by rotating ~~clockwise in order of~~ $\psi_x^{i,0}$, $\psi_y^{i,0}$ and $\psi_z^{i,0}$ about axis- X , Y and Z , respectively, one can transform $X_i Y_i Z_i$ to
 $X_0 Y_0 Z_0$. To realize the coordinate transformation between ~~these/these~~ three coordinate systems, a coordinate rotation matrix
 $A_R(\psi_x, \psi_y, \psi_z)$ is introduced. Using A_R , one can transform the coordinate point or vector presentation from one coordinate
 system to another. The details of the coordinate rotation matrix $A_R(\psi_x, \psi_y, \psi_z)$ can be seen/found in Appendix (A.1).

175 2.3 ~~two~~Two types of measuring errors

The analytical method of the spatial resolution ~~of~~ for each radar link is the same. The difference between ~~these/these~~ radar links
~~are/is~~ only the value of the six ~~coordinates/coordinate~~ rotation ~~angle/angles~~ ($\psi_x^{X,i}$, $\psi_y^{Y,i}$ and $\psi_z^{Z,i}$; $\psi_x^{i,0}$, $\psi_y^{i,0}$ and $\psi_z^{i,0}$) and the
 baseline distance d_i . The spatial resolution related measurement errors which will cause location errors of the MTSP, can be
 classified into two types: E_1 is caused by measurement errors ~~in/at~~ the receiver, and E_2 is due to the pulse length. These two
 180 errors are mutually independent. Hence, the total error (E_{total}) can be expressed as:

$$E_{total}^2 = E_1^2 + E_2^2 \quad (2)$$

E_1 is related to three indirect measuring errors. They are zenith, azimuth and radial distance measuring errors, denoted as $\delta\theta$,
 $\delta\phi$ and δR_s respectively. In XYZ, E_1 can be decomposed into three orthogonal error vectors using $\delta\theta$, $\delta\phi$ and δR_s (see
 figure 4(c)). ~~Now~~) which we ~~now~~ explain ~~it~~ in ~~more~~ detail. PDMEs, i.e., $\delta(\Delta\Psi_1)$ and $\delta(\Delta\Psi_2)$, are caused by some practical
 185 factors, such as phase calibration mismatch and the fact that the specular point is not actually a point but ~~has/is~~ a few Fresnel
 zones ~~in~~ length. A meteor radar system calculates phase ~~difference-of/differences between~~ different ~~pair/pairs~~ of antennas though
 cross-correlations and then ~~fit/fits~~ them to get the most likely AoAs. Therefore, the system needs to ~~set/be assigned~~ a
~~tolerant/tolerance~~ value of $\delta(\Delta\Psi_1)$ and $\delta(\Delta\Psi_2)$. Different meteor radar systems have different ~~AoAs/AoA~~-fit algorithms and
 thus different ~~AoAs/AoA~~ measuring error ~~distribution-distributions~~. To ~~analyse/analyze~~ the spatial resolution for a SIMO

190 meteor radar system as ~~common~~generally as possible and to avoid tedious error propagation ~~in receiver at the receiving array,~~ we start the error propagation from $\delta(\Delta\Psi_1)$ and $\delta(\Delta\Psi_2)$ and set them as ~~constant. AoA~~constants. AoA measuring errors; ~~i.e.~~ $\delta\theta$ and $\delta\phi$ can then be expressed as:

$$\delta\theta = \frac{\lambda}{2\pi D_1} \frac{\cos\phi}{\cos\theta} \delta(\Delta\Psi_1) + \frac{\lambda}{2\pi D_2} \frac{\sin\phi}{\cos\theta} \delta(\Delta\Psi_2) \quad (3)$$

$$\delta\phi = \frac{\lambda}{2\pi D_2} \frac{\cos\phi}{\sin\theta} \delta(\Delta\Psi_2) - \frac{\lambda}{2\pi D_1} \frac{\sin\phi}{\sin\theta} \delta(\Delta\Psi_1) \quad (4)$$

195 where λ is the radio ~~wave length~~wavelength, D_1 and D_2 are the length of the two orthogonal antenna arms, and θ and ϕ are the zenith angle and the azimuth angle, respectively. The details can be ~~seen found~~ in **Appendix (A.2)**. It is worth noting that $\delta\theta$ and $\delta\phi$ are not mutually independent. The ~~Expectation~~expectation value of their product is not identical to zero unless $\frac{E(\delta^2(\Delta\Psi_1))}{D_1^2}$ is equal to $\frac{E(\delta^2(\Delta\Psi_2))}{D_2^2}$.

δR_s can be expressed as a function of δR , $\delta\theta$ and $\delta\phi$ as:

$$200 \quad \delta R_s = F(\delta R, \delta\theta, \delta\phi) = f_R(\theta, \phi)\delta R + f_\theta(\theta, \phi)\delta\theta + f_\phi(\theta, \phi)\delta\phi \quad (5)$$

$f_R(\theta, \phi)$, $f_\theta(\theta, \phi)$ and $f_\phi(\theta, \phi)$ are the weightweighting functions of δR_s . The details about the weightweighting function and deduction can be found in **Appendix (A.3)**. SeeInspection of figure 4(c) indicates that E_1 can be decomposed into three orthogonal error vectors in coordinate XYZ, denoted as $\overrightarrow{\delta R_s}$, $\overrightarrow{R_s\delta\theta}$ and $\overrightarrow{R_s\sin\theta\delta\phi}$. These three vectors can be expressed in XYZ as:

$$205 \quad \overrightarrow{\delta R_s} = \delta R_s(\sin\theta\cos\phi, \sin\theta\sin\phi, \cos\theta)^T \quad (6)$$

$$\overrightarrow{R_s\delta\theta} = R_s\delta\theta(\cos\theta\cos\phi, \cos\theta\sin\phi, -\sin\theta)^T \quad (7)$$

$$\overrightarrow{R_s\sin\theta\delta\phi} = R_s\sin\theta\delta\phi(-\sin\phi, \cos\phi, 0)^T \quad (8)$$

E_2 is related to the radio wave propagatingpropagation path. A pulse might be reflected anywhere within a pulse length (see figure 4(b)). This causes a location error ~~o~~in the MTSP, represented as an error vector $\overrightarrow{D\bar{A}}$. D is the median point of the isosceles triangle ΔABC 's side BC. The representation of the error vector $\overrightarrow{D\bar{A}}$ can be solved in $X_i Y_i Z_i$ by using geometryrelationshipgeometrical relationships as:

$$\overrightarrow{D\bar{A}} = \left(\frac{(2-a_1-a_2)x_1+d_1(a_2-1)}{2}, \frac{(2-a_1-a_2)y_1}{2}, \frac{(2-a_1-a_2)z_1}{2} \right)^T \quad (9)$$

where S is the half wave pulse length and $a_1 = \frac{R_s-S}{R_s}$, $a_2 = \frac{R_i-S}{R_i}$. d_1 is the baseline length. (x_i, y_i, z_i) is the coordinate value of a MTSP (~~i.e.~~ point A in figure 4) in $X_i Y_i Z_i$. DetailsMore details can be ~~seen found~~ in **Appendix (A4)**

215 **2.4 transform Transformation to ENU coordinatecoordinates**

HereThus far, two types of errors in different coordinate systems have been introduced. Now they need to be transformed to ENU coordinates $X_0Y_0Z_0$, which is convenient for comparing between in order to compare different radar linklinks and analysing to analyse the wind fields. E_1 related error vectors, which are three orthogonal vectors $\overline{\delta R_s}$, $\overline{R_s \delta \theta}$ and $\overline{R_s \sin \theta \delta \phi}$ and represented in XYZ as eq.(6)-(8), and need to be transformed from XYZ to $X_0Y_0Z_0$. To project $\overline{\delta R_s}$, $\overline{R_s \delta \theta}$ and $\overline{R_s \sin \theta \delta \phi}$ towards axis- X_0, Y_0, Z_0 respectively, and reassemble them to form three new error vectors in axis- X_0, Y_0, Z_0 . Using the coordinate rotation matrix $A_R^{(XYZ, X_0Y_0Z_0)} = A_R(\Psi_x^{i,0}, \Psi_y^{i,0}, \Psi_z^{i,0}) \cdot A_R(\psi_x^{Y,i}, \psi_y^{Y,i}, \psi_z^{Z,i})$ and eq.(6)-(8), the unit vectors of those three vectors can be represented in $X_0Y_0Z_0$ as:

$$\begin{pmatrix} X'_0(\delta R_s) & X'_0(\delta \theta) & X'_0(\delta \phi) \\ Y'_0(\delta R_s) & Y'_0(\delta \theta) & Y'_0(\delta \phi) \\ Z'_0(\delta R_s) & Z'_0(\delta \theta) & Z'_0(\delta \phi) \end{pmatrix} = A_R^{(XYZ, X_0Y_0Z_0)} \cdot \begin{pmatrix} \sin \theta \cos \phi & \cos \theta \cos \phi & -\sin \phi \\ \sin \theta \sin \phi & \cos \theta \sin \phi & \cos \phi \\ \cos \theta & -\sin \theta & 0 \end{pmatrix} \quad (10)$$

$(X'_0(\delta R_s), Y'_0(\delta R_s), Z'_0(\delta R_s))^T$, $(X'_0(\delta \theta), Y'_0(\delta \theta), Z'_0(\delta \theta))^T$, $(X'_0(\delta \phi), Y'_0(\delta \phi), Z'_0(\delta \phi))^T$ are unit vectors of $\overline{\delta R_s}$, $\overline{R_s \delta \theta}$ and $\overline{R_s \sin \theta \delta \phi}$ in $X_0Y_0Z_0$ respectively. The 3×3 matrix in on the left hand side of the eq.(10) is denoted as P_{ij} for $i, j = 1, 2, 3$.

SeeFrom eq.(6)-(8) and figure 4(c), we see that the length of those three vectors, or (the error values in other words,) are δR_s , $R_s \delta \theta$, $R_s \sin \theta \delta \phi$ as thea function of δR , $\delta \theta$, $\delta \phi$. In order to reassemble them to form new error vectors, transforming transformation of $\delta \theta$ and $\delta \phi$ into two independent errors $\delta(\Delta \Psi_1)$ and $\delta(\Delta \Psi_2)$ are is needed because $\delta \theta$ and $\delta \phi$ are not independent. Using eq. (3) and (4), one can transform vector $(\delta R, \delta \theta, \delta \phi)^T$ to three independent measuring errors δR , $\delta(\Delta \Psi_1)$ and $\delta(\Delta \Psi_2)$. And thus $(\delta R_s, R_s \delta \theta, R_s \sin \theta \delta \phi)^T$ can be expressed as:

$$\begin{pmatrix} \delta R_s \\ R_s \delta \theta \\ R_s \sin \theta \delta \phi \end{pmatrix} = \begin{pmatrix} f_R(\theta, \phi) & f_\theta(\theta, \phi) & f_\phi(\theta, \phi) \\ 0 & R_s & 0 \\ 0 & 0 & R_s \sin \theta \end{pmatrix} \cdot \begin{pmatrix} 1 & 0 & 0 \\ 0 & \frac{\lambda}{2\pi} \cos \phi & \frac{\lambda}{2\pi} \sin \phi \\ 0 & \cos \theta D_1 & \cos \theta D_2 \\ 0 & -\frac{\lambda}{2\pi} \sin \phi & \frac{\lambda}{2\pi} \cos \phi \\ 0 & \sin \theta D_1 & \sin \theta D_2 \end{pmatrix} \cdot \begin{pmatrix} \delta R \\ \delta(\Delta \Psi_1) \\ \delta(\Delta \Psi_2) \end{pmatrix} \quad (11)$$

The product of the first and the second term in on the right hand side of eq.(11) is a 3×3 matrix, denoted as W_{ij} for $i, j = 1, 2, 3$. SeenFrom eq.(11), we see that the three error values values δR_s , $R_s \delta \theta$, $R_s \sin \theta \delta \phi$ are the linear combinations of three basis δR , $\delta(\Delta \Psi_1)$, and $\delta(\Delta \Psi_2)$ with their corresponding linear coefficients W_{1j}, W_{2j}, W_{3j} and W_{3j} . Those three error values can be projected toward new directions (i.e. g., axis- X_0, Y_0, Z_0) by using P_{ij} . It worth noting that in a new direction, a same basis's projected linear coefficients from different error values should be used to calculate their sum of squares (SS). And then the square root of SS will be used as a new linear coefficient for that basis in the new direction. For example, in X_0 directions, basis $\delta(\Delta \Psi_1)$'s projected linear coefficients are $X'_0(\delta R_s)W_{12}$, $X'_0(\delta \theta)W_{22}$, $X'_0(\delta \phi)W_{32}$ from $\overline{\delta R_s}$, $\overline{R_s \delta \theta}$ and $\overline{R_s \sin \theta \delta \phi}$ respectively. Therefore, the new linear coefficient for $\delta(\Delta \Psi_1)$ in the X_0 direction is $W_{X'_0}^{\delta(\Delta \Psi_1)} =$

$\pm\sqrt{(X'_0(\delta R_s)W_{12})^2 + (X'_0(\delta\theta)W_{22})^2 + (X'_0(\delta\phi)W_{32})^2}$. Similarly, one can get δR and $\delta(\Delta\Psi_2)$'s new linear coefficients in X'_0 , denoted as $W_{X'_0}^{\delta R}$ and $W_{X'_0}^{\delta(\Delta\Psi_2)}$. Thus, the true error values in the X_0 direction is $W_{X'_0}^{\delta R}\delta R + W_{X'_0}^{\delta(\Delta\Psi_1)}\delta(\Delta\Psi_1) + W_{X'_0}^{\delta(\Delta\Psi_2)}\delta(\Delta\Psi_2)$. Because δR , $\delta(\Delta\Psi_1)$, and $\delta(\Delta\Psi_2)$ are mutually independent, E_1 is related to the mean square error (MSE) values in the X_0 direction, denoted as $\delta_{(1)}X_0$, and can be expressed as $\delta_{(1)}X_0 =$

$$245 \quad \pm\sqrt{\left(W_{X'_0}^{\delta R}\delta R\right)^2 + \left(W_{X'_0}^{\delta(\Delta\Psi_1)}\delta(\Delta\Psi_1)\right)^2 + \left(W_{X'_0}^{\delta(\Delta\Psi_2)}\delta(\Delta\Psi_2)\right)^2}.$$

In short, E_1 related errors in ENU coordinate's three axis directions (denoted as $\delta_{(1)}X_0$, $\delta_{(1)}Y_0$ and $\delta_{(1)}Z_0$) can be expressed in the form of a matrix as:

$$\begin{pmatrix} \delta_{(1)}^2 X_0 \\ \delta_{(1)}^2 Y_0 \\ \delta_{(1)}^2 Z_0 \end{pmatrix} = P_{ij}^2 \cdot W_{ij} \cdot \begin{pmatrix} \delta^2 R \\ \delta^2(\Delta\Psi_1) \\ \delta^2(\Delta\Psi_2) \end{pmatrix} \quad (12)$$

250 The E_2 related error vector \overrightarrow{DA} needs transformation from $X_i Y_i Z_i$ to $X_0 Y_0 Z_0$. Therefore, E_2 related errors in the ENU coordinate's three axis directions (denoted as $\delta_{(2)}X_0$, $\delta_{(2)}Y_0$ and $\delta_{(2)}Z_0$) can be expressed in the form of a matrix as:

$$\begin{pmatrix} \delta_{(2)} X_0 \\ \delta_{(2)} Y_0 \\ \delta_{(2)} Z_0 \end{pmatrix} = \pm A_R(\Psi_x^{i,0}, \Psi_y^{i,0}, \Psi_z^{i,0}) \cdot \overrightarrow{DA} \quad (13)$$

E_1 and E_2 are mutually independent. By using eq.(1), the total MSE values in ENU coordinate's three axis directions (denoted as $\delta_{\text{total}}X_0$, $\delta_{\text{total}}Y_0$ and $\delta_{\text{total}}Z_0$) can be expressed in the form of matrix as:

$$\begin{pmatrix} \delta_{\text{total}}^2 X_0 \\ \delta_{\text{total}}^2 Y_0 \\ \delta_{\text{total}}^2 Z_0 \end{pmatrix} = \begin{pmatrix} \delta_{(1)}^2 X_0 \\ \delta_{(1)}^2 Y_0 \\ \delta_{(1)}^2 Z_0 \end{pmatrix} + \begin{pmatrix} \delta_{(2)}^2 X_0 \\ \delta_{(2)}^2 Y_0 \\ \delta_{(2)}^2 Z_0 \end{pmatrix} \quad (14)$$

255 In conclusion, for a radar link L_i and a MTSP represented as (x_0, y_0, z_0) in the ENU coordinate system $X_0 Y_0 Z_0$, as sketched in figure 4(a) sketched, the location errors of this point in east, north and up directions ($\pm\delta_{\text{total}}X_0$, $\pm\delta_{\text{total}}Y_0$ and $\pm\delta_{\text{total}}Z_0$) can be calculated as follows: firstly, for a point (x_0, y_0, z_0) in $X'_0 Y'_0 Z'_0$, using A_R to transform it to $X_i Y_i Z_i$ and denoted as (x_i, y_i, z_i) . Then in $X_i Y_i Z_i$ calculate AoA (θ and ϕ) and the range information (R_s and R_i). Details of AoA and range calculation can be seen in **Appendix (A.5)**. It's worth noting that AoA is given by the angles relative to axis of XYZ. Secondly, in XYZ using AoA and eq.(3)-(8) to calculate E_1 's three orthogonal error vectors as shown in figure 4(c) sketched; in $X_i Y_i Z_i$ use the range information and eq.(9) to calculate E_2 's error vector \overrightarrow{DA} as shown in figure 4(b) sketched. Thirdly, project E_1 's three error vectors to $X_0 Y_0 Z_0$ by using eq.(10) and use eq.(11)-(12) to reassemble them to calculate E_1 related MSE values in the direction of

265 X_0, Y_0, Z_0 ; use eq.(13) to transform the E_2 error vector from $X_i Y_i Z_i$ to $X_0 Y_0 Z_0$. Finally, use eq. (14) to get the total location errors of a MTSP in (x_0, y_0, z_0) . Figure 5(a) describesshows the flow chart for the process above.—we have just described.

3 Results and Discussion

~~We wrote a~~The program to study the method we have described above.~~The program~~ is written in the python language and is presented in the supplement. To calculate a special configuration of a multistatic radar system, we initially need to set six coordinate transformation angles ($\psi_x^{X,i}$, $\psi_y^{Y,i}$ and $\psi_z^{Z,i}$; $\psi_x^{i,0}$, $\psi_y^{i,0}$ and $\psi_z^{i,0}$) and the baseline length (~~i.e. d_i~~) for each radar link
270 L_i . For example: $\psi_x^{i,0} = \psi_y^{i,0} = 0$, $\psi_z^{i,0} = 30^\circ$ and $d_i = 250\text{km}$ means at that transmitter T_i is 250km250 km, 30° east by south of the receiver R_X ; Further, $\psi_x^{X,i} = 5^\circ$, $\psi_y^{Y,i} = 0$, $\psi_z^{Z,i} = 0$ means one receiver arm (axis-Y) points to east by north 60° with 5° elevation. The ~~interested~~ detection area of interest for a multistatic meteor radar is usually from 70km70 km to 110km110 km in height and larger thanaround $300\text{km} \times 300\text{km}$ in the horizontal. In our program, this area needs to be divided into a spatial grid for sampling. The default value of the sampling grid length is 1km1 km in height and 5km5 km in ~~meridian~~the
275 meridional and zonal directions, respectively. After selecting the desired settings ~~mentioned above~~, the program ~~will traverse those steps though the~~ sampling grid nodes and calculatecalculates the location errors ~~of at~~ each ~~nodesnode~~ as described in figure 5(a). Figure 5(b) describedescribes the parameter settings and ~~traversalthe transversal~~ calculation process ~~above~~. For a given setting of radar link L_i , the program will output the squared values of E_1 related, E_2 related and total MSE (E_{total}^2 : $\delta_{total}^2 X_0$, $\delta_{total}^2 Y_0$, $\delta_{total}^2 Z_0$; E_1^2 : $\delta_{(1)}^2 X_0$, $\delta_{(1)}^2 Y_0$, $\delta_{(1)}^2 Z_0$; E_2^2 : $\delta_{(2)}^2 X_0$, $\delta_{(2)}^2 Y_0$, $\delta_{(2)}^2 Z_0$). The location errors can be positive
280 or negative and thus the spatial resolutions are twice the absolute value of the location errors. For an example, Seesee figure 5(c), ~~for~~. For a detected MTSP represented as (x_0, y_0, z_0) in $X_0 Y_0 Z_0$, ifwith $\delta_{total}^2 X_0$, $\delta_{total}^2 Y_0$, $\delta_{total}^2 Z_0$ equalsequal to 25, 16 and 9 km^2 respectively, ~~it means that~~ the actual position of the MTSP could occur in an area which is ± 5 km, ± 4 km, ± 3 km around (x_0, y_0, z_0) with equallyequal probability. TheConsequently, the zonal, ~~meridian~~meridional and vertical ~~resolution~~resolutions are 10 km, 8 km and 6 km respectively.
285 The HM analyses the vertical resolution (corresponding to δZ_0 in our paper) ~~only~~ in a 2-dimensional vertical section (corresponding to the $X_0 Z_0$ plane in our paper). To compare with Hocking's work, ~~except~~ $\psi_z^{i,0}$ is set to ~~be~~ 180° , and the other five coordinate transformation angles are all set to zero with d is equal to 300 km. The half wave pulse length S is set to 2 km and $\delta(\Delta\Psi_1)$ to 35° . Calculating in ~~only~~ the $X_0 Y_0$ plane only should have degraded our method into Hocking's 2-dimensional analysis method, but ~~the settings above~~ doesn't work because Hocking'sthe HM method ignores δR_s . In fact,
290 Hocking's methodthe HM considers only E_2 and $\overline{R_s \delta\theta}$ in the $X_0 Y_0$ plane. HenceConsequently, we need to further set $f_R(\theta, \phi)$, $f_\theta(\theta, \phi)$ and $f_\phi(\theta, \phi)$ to be zero. ThusWhen this is done, our method totally degrades into Hocking's methodthe HM. Hocking's results are shown in the absolute value of vertical location error normalized relative to the half wave pulse width, ~~i.e.~~ $|\delta Z_0|/S$. HereafterHereinafter, $|E|/S$ is referred to as the normalized spatial ~~resolutions~~resolution such as $\delta_{(1)} X_0$

and $\delta_{total}Y_0$, where E represents the location errors in a direction. Thus, the spatial resolutions are 2S times the normalized spatial resolutions. The

Our normalized vertical resolution distributions are shown in figure 6(a). Our results and are the same as those presented in Hocking's work (Hocking, 2018). The distribution of $\overline{R_s\delta\theta}$ related, E_2 related, and total normalized vertical resolution distributions are shown in figure 6 from left to right, respectively. In most cases, E_2 is an order of magnitude smaller than $\overline{R_s\delta\theta}$. Only in the region directly above the receiver does E_2 have the same magnitude as $\overline{R_s\delta\theta}$. In other words, only in the region directly above the receiver can E_2 influence the total resolution. E_2 is related to the bistatic configuration, but $\overline{R_s\delta\theta}$ is not. Therefore, in the HM, the distribution of the total vertical resolution is changed/changes slightly with \mathbf{d} . After adding the error term $\overline{\delta R_t}$, which is related to the bistatic configuration, the normalized total vertical spatial resolution distribution will change visibly/changes more obviously with \mathbf{d} , as figure 7's first two rows show. The region between the two black lines represents a trustworthy/the sampling volume for the receiver because/where the elevation angle is beyond 30° with less influence of potential mutual antenna coupling or other obstacles in the surrounding. However, with As the transmitter/receiver distance become longer, resolutions in this trustworthy sampling volume are not always acceptable. In figure 7's first row, the transmitter/receiver distance is 300 km and about half of the region between two black line have normalized vertical resolution values larger/larger than 3 km. Because our analytical method can obtain spatial resolutions in 3-dimensional space, figure 7's third row shows/shows a perspective to the horizontal section at 90 km altitude for figure 7's second row.

To get an intuitionistic-a perspective on the spatial resolution distribution in 3-dimensional space, figure 8 shows the normalized zonal, meridian/meridional and vertical spatial resolution distribution of/distributions for a multistatic radar link whose transmitter/receiver separation is 180 km away and the transmitter is south by east 30° of the receiver. Classic/The classic monostatic meteor radar is a special case of a multistatic meteor radar system whose baseline length is zero. By setting the transmitter/receiver distance to be zero in our program, a monostatic meteor radar's spatial resolution can also be obtained. The/In this case, the spatial resolution distributions are highly symmetrical and correspond to the real characteristics of monostatic meteor radar (this is not shown in the text here, but can be seen/found in the supplement SF1). In the discussion above, the receiver and transmitter antennas are all coplanar. By setting/varying $\psi_x^{x,i}$, $\psi_y^{y,i}$ and $\psi_z^{z,i}$ in our program, the non-coplanar receiver/transmitter-antennas situations can also be studied. Slightly tilting of the receiver horizontal plane (for example, set $\psi_x^{x,i}=\psi_y^{y,i}=5^\circ$) will cause/causes the horizontal spatial distributions to change (see/see SF2 and SF3 in the supplement). In practical applications, like/practice, the Earth's curvature and local topography will lead to tilts in the receiver horizontal plane-tilting. Thus, this. This kind of tilting/tilt should also be taken into account for multistatic meteor radar systems. The and details of relating to the parameter setting selections for this can be seen/found in the supplement.

The AoAs/AoA error propagation process in the receiver has been simplified to yield eq.(3)-(4) by using the constant PDMEs as the start of error propagation. This is for the sake of the adaptable/providing the most general example of our method. If analysing AoA/the analysis of AoA errors starts/were to start from the original received voltage signals; (e.g., Vaudrin et al.,

2018), the error propagation process ~~will change with a~~ would depend on the specific receiver interferometer configuration and ~~the~~ specific signal processing method. ~~In practical situations for an unusual~~ The approach used here can be applied to different receiver antenna ~~configuration~~ configurations or new ~~original~~ signal processing algorithm, ~~an error propagation process based on the specific circumstances needs to be established. Substitute~~ algorithms. This would involve substitution of $\delta(\Delta\Psi_1)$ and $\delta(\Delta\Psi_2)$ into other mutually independent measuring errors ~~in a practical situation, to suit the experimental arrangement~~ and then establishing a new ~~AoAsAoA~~ error propagation to obtain $\delta\theta$ and $\delta\phi$. ~~Or in other words, rewrite~~ This means rewriting the second and third term in eq. (11) to the ~~determine a~~ new ~~established AoAsAoA~~ error propagation matrix and new mutually independent measuring errors, respectively. ~~Our analytical method can still work.~~

335 It worth noting that except ~~for using~~ the PDMEs as the start of the error propagation, all the analytical processes are built on ~~the mathematic~~ mathematical error propagations. PDMEs include ~~the~~ uncontrolled errors, such as ~~the those resulting from the returned wave being~~ scattered ~~wave~~ from a few Fresnel zones along ~~the~~ meteor ~~trail~~ trail, phase calibration inaccuracy, and ~~noises~~ noise. However, there are other error sources in ~~practical situation, practice~~. For example, ~~planes~~ aircraft or lightning ~~may make troubles for meteor radar's discrimination system. And~~ interference ~~of and fading clutter from~~ obstacles ~~in surroundings~~ will ~~can~~ cause further measurement errors ~~of AoAs in the AoA~~. These issues are related to actual physical situations and beyond the scope of this text.

~~The trustworthy sampling volume~~ Knowing the valid observational volume for meteor detections and the errors associated ~~with each detection~~ is vital for a meteor radar system ~~and as~~ it determines ~~the detection area and~~ which meteors ~~could~~ can be used ~~into calculate~~ wind ~~retrievals, velocities and also the uncertainties associated with the winds themselves~~. To ~~avoid~~ reduce the influence of ~~the~~ mutual antenna coupling or ~~the~~ ground clutter, the elevation angle of a detection should ~~beyond~~ be above a threshold, ~~for example and~~ 30° ~~in general~~. ~~The spatial resolution is another thing that affects the trustworthy sampling typically used, and this sets the basic valid observational~~ volume. ~~See~~ Within this, the normalised vertical resolution ~~varies, and in~~ Figure 7 and SF4 in ~~the~~ supplement, only the ~~area~~ areas of normalized vertical resolution ~~with~~ values below 3 km are shown, which ~~we argue~~ represents an acceptable sampling volume. ~~With~~ In addition, as ~~the~~ transmitter/receiver distance ~~increasing, this increases, the~~ sampling volume becomes smaller ~~along with and~~ the vertical resolution in this volume ~~is~~ reduced. This ~~fact~~ effect limits the ~~practically usable~~ transmitter/receiver ~~distance~~ distances for multistatic meteor ~~radar. Measurement response is important for measuring meteor trails' Doppler shift caused by the background wind. The radars.~~

~~The geometry of the multistatic meteor radar case also impacts on the ability of the radar to measure the Doppler shifts associated with drifting meteor trails within the observational volume. This is because the~~ measured Doppler shift is ~~caused~~ produced by the component of the wind ~~fields~~ field in ~~the direction of~~ the Bragg Vector-, ~~which in the multistatic configuration is divergent from the receiver's line of sight (see e.g., Spargo et al., 2019).~~ The smaller the angle between ~~the~~ Bragg vector and the wind fields ~~is~~, the ~~larger this~~ larger is the Doppler shift ~~is~~ (and ~~meanwhile~~ the higher SNR. ~~The Bragg vector of the multistatic configuration is divergent from the receiver's line of sight. Monostatic meteor radars can only detect winds in radial direction, thus only the mean wind can be solved. By synthesizing monostatic and multistatic the high order component of the wind fields can be solved. The bigger the angle between the Bragg vector and radial direction is, or more~~

diversified Bragg vectors in other words, the more complete and accurate the wind fields will be observed. In short, the trustworthy sampling volume, measurement response and the SNR). This means that within the observational volume, the angular diversity of the Bragg vector should both be taken into account in the wind retrievals. The retrieval process. A discussion of wind retrievals is beyond the scope of this text and will be considered in a future work.

365

4 Conclusion

In this study, we have presented the preliminary results of our from an analytical error analytic method. Our analysis of multistatic meteor radar system measurements of angles of arrival. The method can calculate the spatial resolution (the spatial uncertainty) in the zonal, meridian meridional and vertical direction directions for an arbitrary receiving antenna array configuration in three-dimensional space. A given detected MTSP can locate is located within the spatial resolution volume with an equal probability. Higher values of spatial resolution mean that this region needs more meteor counts or longer averaging to obtain a reliable accuracy. Our method shows that the spatial configuration of a multistatic system will greatly influence the spatial resolution distribution in ENU coordinates and thus will in turn influence the retrieval accuracy of atmospheric parameters such as the wind fields field. The multistatic meteor radar system's spatial resolution analysis is a key point in analysing the accuracy of retrieved wind and other parameters. The influence of the spatial resolutions resolution on wind retrieval will be discussed in the future work.

370

375

Multistatic radar systems come in many types, and our the work in this paper considers only single-input (single-antenna transmitter) and multi-output (5-antenna interferometric receiver) pulse radar systems. Although the single-input multi-output (SIMO) pulse meteor radar is a classic meteor radar system, other meteor radar systems, such as continuous wave radar systems and MISO (multiple-antenna transmitter and single-antenna receiver), also show good experimental results and have some advantages over SIMO systems. Using different types of meteor radar systems to constitute the meteor radar network is the future trend and so we will add the spatial resolution analyses analysis of other system to the frame of types using our method in the future. We will also validate and apply the error analyses of spatial resolution analysis in the horizontal wind determination into a multistatic meteor radar system, which that will be built soon be installed in China.

380

385

Code availability. The program to calculate the 3D spatial resolution distributions are is available in the supplement.

Author contributions: W.Z, X.X, W.Y designed the study. W.Z deduced the formulas and wrote the program. W.Z wrote the paper for the first version. X.X supervised the work and provided valuable comments. I.M.R revised the paper. All of the authors discussed the results and commented on the paper.

390

Competing interest. The authors declare no conflicts of interests

Acknowledgements. This work is supported by the B-type Strategic Priority Program of CAS Grant No. XDB41000000, the
395 National Natural Science Foundation of China (41774158, 41974174, 41831071 and 41904135), the CNSA pre-research
Project on Civil Aerospace Technologies No. D020105, the Fundamental Research Funds for the Central Universities, and the
Open Research Project of Large Research Infrastructures of CAS “Study on the interaction between low/mid-latitude
atmosphere and ionosphere based on the Chinese Meridian Project.” ~~Thanks for~~WZ thanks Dr. Jia Mingjiao ~~to provide~~
~~advises~~for useful discussions and Zeng ~~jie to check~~Jie for checking the equations in ~~this~~the manuscript.

400 Reference

- Browning, K. A., and Wexler, R.: The Determination of Kinematic Properties of a Wind Field Using Doppler Radar, *Journal of Applied Meteorology*, 7, 105-113, 10.1175/1520-0450(1968)007<0105:Tdokpo>2.0.Co;2, 1968.
- Ceplecha, Z., Borovička, J., Elford, W. G., ReVelle, D. O., Hawkes, R. L., Porubčan, V., and Šimek, M.: Meteor Phenomena and Bodies, *Space Science Reviews*, 84, 327-471, 10.1023/A:1005069928850, 1998.
- 405 Chau, J. L., Stober, G., Hall, C. M., Tsutsumi, M., Laskar, F. I., and Hoffmann, P.: Polar mesospheric horizontal divergence and relative vorticity measurements using multiple specular meteor radars, *Radio Science*, 52, 811-828, 10.1002/2016rs006225, 2017.
- Chau, J. L., Urco, J. M., Vierinen, J. P., Volz, R. A., Clahsen, M., Pfeffer, N., and Trautner, J.: Novel specular meteor radar systems using coherent MIMO techniques to study the mesosphere and lower thermosphere, *Atmos. Meas. Tech.*, 12, 2113-2127, 10.5194/amt-12-2113-2019, 2019.
- 410 DOREY, J., BLANCHARD, Y., and CHRISTOPHE, F.: Le projet RIAS, une approche nouvelle du radar de surveillance aérienne, *Onde électrique*, 64, 15-20, 1984.
- Hocking, W. K., Fuller, B., and Vandeppeer, B.: Real-time determination of meteor-related parameters utilizing modern digital technology, *Journal of Atmospheric and Solar-Terrestrial Physics*, 63, 155-169, 10.1016/s1364-
415 6826(00)00138-3, 2001.
- Hocking, W. K.: Spatial distribution of errors associated with multistatic meteor radar, *Earth, Planets and Space*, 70, 93, 10.1186/s40623-018-0860-2, 2018.
- Holdsworth, D. A., Reid, I. M., and Cervera, M. A.: Buckland Park all-sky interferometric meteor radar, *Radio Science*, 39, 10.1029/2003rs003014, 2004.
- 420 Jacobi, C., Hoffmann, P., and K¹rschner, D.: Trends in MLT region winds and planetary waves, *Collm (52jã N, 15jã E), Annales Geophysicae (ANGEO)*, 2008.
- Jia, M. J., Xue, X. H., Dou, X. K., Tang, Y. H., Yu, C., Wu, J. F., Xu, J. Y., Yang, G. T., Ning, B. Q., and Hoffmann, L.: A case study of A mesoscale gravity wave in the MLT region using simultaneous multi-instruments in Beijing, *Journal of Atmospheric and Solar-Terrestrial Physics*, 140, 1-9, 10.1016/j.jastp.2016.01.007, 2016.
- 425 Jones, J., Webster, A. R., and Hocking, W. K.: An improved interferometer design for use with meteor radars, *Radio Science*, 33, 55-65, 10.1029/97rs03050, 1998.
- Kang, C.: Meteor radar signal processing and error analysis, 2008.
- Philippe, W., and Corbin, H.: On the Analysis of Single-Doppler Radar Data, *Journal of Applied Meteorology - J APPL METEOROL*, 18, 532-542, 10.1175/1520-0450(1979)018<0532:OTAOSD>2.0.CO;2, 1979.

- 430 Reid, I. M.: SOME ASPECTS OF DOPPLER RADAR MEASUREMENTS OF THE MEAN AND FLUCTUATING COMPONENTS OF THE WIND-FIELD IN THE UPPER MIDDLE ATMOSPHERE, *Journal of Atmospheric and Terrestrial Physics*, 49, 467-484, 10.1016/0021-9169(87)90041-9, 1987.
- Spargo, A. J., Reid, I. M., and MacKinnon, A. D.: Multistatic meteor radar observations of gravity-wave-tidal interaction over southern Australia, *Atmos. Meas. Tech.*, 12, 4791-4812, 10.5194/amt-12-4791-2019, 2019.
- 435 Stober, G., Sommer, S., Rapp, M., and Latteck, R.: Investigation of gravity waves using horizontally resolved radial velocity measurements, *Atmos. Meas. Tech.*, 6, 2893-2905, 10.5194/amt-6-2893-2013, 2013.
- Stober, G., and Chau, J. L.: A multistatic and multifrequency novel approach for specular meteor radars to improve wind measurements in the MLT region, *Radio Science*, 50, 431-442, 10.1002/2014rs005591, 2015.
- Stober, G., Chau, J. L., Vierinen, J., Jacobi, C., and Wilhelm, S.: Retrieving horizontally resolved wind fields using multi-
- 440 static meteor radar observations, *Atmos. Meas. Tech.*, 11, 4891-4907, 10.5194/amt-11-4891-2018, 2018.
- Urco, J. M., Chau, J. L., Weber, T., Vierinen, J. P., and Volz, R.: Sparse Signal Recovery in MIMO Specular Meteor Radars With Waveform Diversity, *IEEE Transactions on Geoscience and Remote Sensing*, 57, 10088-10098, 10.1109/tgrs.2019.2931375, 2019.
- Vaudrin, C. V., Palo, S. E., and Chau, J. L.: Complex Plane Specular Meteor Radar Interferometry, *Radio Science*, 53, 112 -
- 445 128, 10.1002/2017rs006317, 2018.
- Vierinen, J., Chau, J. L., Pfeffer, N., Clahsen, M., and Stober, G.: Coded continuous wave meteor radar, *Atmospheric Measurement Techniques*, 9, 829-839, 10.5194/amt-9-829-2016, 2016.
- Vierinen, J., Chau, J. L., Charuvil, H., Urco, J. M., Clahsen, M., Avsarkisov, V., Marino, R., and Volz, R.: Observing Mesospheric Turbulence With Specular Meteor Radars: A Novel Method for Estimating Second-Order
- 450 Statistics of Wind Velocity, *Earth and Space Science*, 6, 1171-1195, 10.1029/2019ea000570, 2019.
- Xue, X. H., Dou, X. K., Lei, J., Chen, J. S., Ding, Z. H., Li, T., Gao, Q., Tang, W. W., Cheng, X. W., and Wei, K.: Lower thermospheric-enhanced sodium layers observed at low latitude and possible formation: Case studies, *Journal of Geophysical Research-Space Physics*, 118, 2409-2418, 10.1002/jgra.50200, 2013.
- Yi, W., Xue, X. H., Reid, I. M., Younger, J. P., Chen, J. S., Chen, T. D., and Li, N.: Estimation of Mesospheric Densities at
- 455 Low Latitudes Using the Kunming Meteor Radar Together With SABER Temperatures, *Journal of Geophysical Research-Space Physics*, 123, 3183-3195, 10.1002/2017ja025059, 2018.
- Younger, J. P., and Reid, I. M.: Interferometer angle-of-arrival determination using precalculated phases, *Radio Science*, 52, 1058-1066, 10.1002/2017rs006284, 2017.

460 **Appendix**

A.1 Coordinates rotation matrix

For a right-handed rectangular coordinate system XYZ , we rotate clockwise Ψ_x about the axis-x to obtain a new coordinate. We specify that clockwise rotation satisfies in the right-hand screw rule. A vector in XYZ , denoted as $(x, y, z)^T$, is represented as $(x', y', z')^T$ in the new coordinate. The relationship between $(x, y, z)^T$ and $(x', y', z')^T$ is:

$$465 \begin{pmatrix} x' \\ y' \\ z' \end{pmatrix} = A_x(\psi_x) \begin{pmatrix} x \\ y \\ z \end{pmatrix} = \begin{pmatrix} 1 & 0 & 0 \\ 0 & \cos\psi_x & \sin\psi_x \\ 0 & -\sin\psi_x & \cos\psi_x \end{pmatrix} \begin{pmatrix} x \\ y \\ z \end{pmatrix} \quad (\text{A1.1})$$

Similarly, we rotate clockwise Ψ_y ~~is~~ about the axis-y to obtain a new coordinate. The presentation for a vector in new coordinates and the original can be linked by a matrix, $A_y(\psi_y)$:

$$A_y(\psi_y) = \begin{pmatrix} \cos\psi_y & 0 & -\sin\psi_y \\ 0 & 1 & 0 \\ \sin\psi_y & 0 & \cos\psi_y \end{pmatrix} \quad (\text{A1.2})$$

we rotate clockwise Ψ_z about axis-z to obtain a new coordinate. The presentation for a vector in new coordinates and original
470 can be linked by a matrix $A_z(\psi_z)$:

$$A_z(\psi_z) = \begin{pmatrix} \cos\psi_z & \sin\psi_z & 0 \\ -\sin\psi_z & \cos\psi_z & 0 \\ 0 & 0 & 1 \end{pmatrix} \quad (\text{A1.3})$$

For any two coordinate systems XYZ and $X'Y'Z'$ with co-origin, one can always rotate clockwise Ψ_x , Ψ_y and ψ_z in order of axis-X, Y, Z respectively, transforming XYZ to $X'Y'Z'$ (figure A.1). The presentation for a vector in $X'Y'Z'$ and XYZ can be linked by a matrix, $A_R(\psi_x, \psi_y, \psi_z)$:

$$475 \quad A_R(\psi_x, \psi_y, \psi_z) = A_z(\psi_z)A_y(\psi_y)A_x(\psi_x) = \begin{pmatrix} \cos\psi_y\cos\psi_z & \sin\psi_x\sin\psi_y\cos\psi_z + \cos\psi_x\sin\psi_z & -\cos\psi_x\sin\psi_y\cos\psi_z + \sin\psi_x\sin\psi_z \\ -\cos\psi_y\sin\psi_z & -\sin\psi_x\sin\psi_y\sin\psi_z + \cos\psi_x\cos\psi_z & \cos\psi_x\sin\psi_y\sin\psi_z + \sin\psi_x\cos\psi_z \\ \sin\psi_y & -\sin\psi_x\cos\psi_y & \cos\psi_x\cos\psi_y \end{pmatrix} \quad (\text{A1.4})$$

We call $A_R(\psi_x, \psi_y, \psi_z)$ ~~as~~ the coordinates rotation matrix.

A.2 ~~AoAsAoA~~ measuring errors

In coordinate XYZ , AoAs includes zenith angle θ and azimuth angle ϕ . In the plane wave approximation, the radio wave is
480 at angle γ_1 and γ_2 with an antenna array (figure A.2). There is a phase difference $\Delta\Psi_1$ and $\Delta\Psi_2$ between two antennas (figure 1). See figure 1, $\Delta\Psi_1$ and $\Delta\Psi_2$ can be expressed as:

$$\Delta\Psi_1 = \frac{2\pi D_1 \cos\gamma_1}{\lambda} \quad (\text{A2.1})$$

$$\Delta\Psi_2 = \frac{2\pi D_2 \cos\gamma_2}{\lambda} \quad (\text{A2.2})$$

Using γ_1 , γ_2 the ~~AoAsAoA~~ can be expressed as:

$$485 \quad \cos^2 \gamma_1 + \cos^2 \gamma_2 + \cos^2 \theta = 1 \quad (\text{A2.3})$$

$$\tan\phi = \frac{\cos\gamma_2}{\cos\gamma_1} \quad (\text{A2.4})$$

Or in another expression:

$$\cos\gamma_1 = \sin\theta\cos\phi \quad (\text{A2.5})$$

$$\cos\gamma_2 = \sin\theta\sin\phi \quad (\text{A2.6})$$

490 substitute $\cos\gamma_1$ and $\cos\gamma_2$ in (A2.3) and (A2.4) by using (A2.1) and (A2.2):

$$\cos^2\theta = 1 - \left(\frac{\lambda}{2\pi}\right)^2 \left(\frac{\Delta^2\Psi_1}{D_1^2} + \frac{\Delta^2\Psi_2}{D_2^2}\right) \quad (\text{A2.7})$$

$$\ln(\tan\phi) = \ln(D_1\Delta\Psi_2) - \ln(D_2\Delta\Psi_1) \quad (\text{A2.8})$$

(A2.7) and (A2.8) link the phase difference with the $\Delta\Psi_1$ and $\Delta\Psi_2$ and expanding θ and ϕ , $\Delta\Psi_1$ and $\Delta\Psi_2$ to first order:

$$2\cos\theta\sin\theta\delta\theta = \left(\frac{\lambda}{2\pi}\right)^2 \left[\frac{2\Delta\Psi_1\delta(\Delta\Psi_1)}{D_1^2} + \frac{2\Delta\Psi_2\delta(\Delta\Psi_2)}{D_2^2}\right] \quad (\text{A2.9})$$

$$495 \quad \delta\phi = \frac{\sin\phi\cos\phi}{\Delta\Psi_2} \delta(\Delta\Psi_2) - \frac{\sin\phi\cos\phi}{\Delta\Psi_1} \delta(\Delta\Psi_1) \quad (\text{A2.10})$$

For (A2.9) and (A2.10), substitute $\Delta\Psi_1$ and $\Delta\Psi_2$ using (A2.1), (A2.2) and (A2.5), (A2.6) to the functions of θ , ϕ . Now, eq.

(3) and eq. (4) have been proven. If the zenith angle $\theta = 0^\circ$, we stipulate that $\frac{\cos\phi}{\sin\theta}$ and $\frac{\sin\phi}{\sin\theta}$ are 1.

A.3 Radial distance measuring error

Expand R_s , R and $\cos\alpha$ in eq.(1) to first order, δR_s can be expressed as a function of δR and $\delta(\cos\alpha)$:

$$500 \quad \delta R_s = \frac{R^2 - 2Rd\cos\alpha + d^2}{2(R - d\cos\alpha)^2} \delta R + \frac{d(R^2 - d^2)}{2(R - d\cos\alpha)^2} \delta(\cos\alpha) \quad (\text{A3.1})$$

α is the angle between R_s and axis- X_i . We denote the zenith and azimuth angles in coordinate- $X_i Y_i Z_i$ as θ' and ϕ' , respectively. And the relationship between α and θ' , ϕ' is

$$\cos\alpha = \sin\theta' \cos\phi' \quad (\text{A3.2})$$

Using coordinates rotation matrix $A_R(\psi_x^{X,i}, \psi_y^{Y,i}, \psi_z^{Z,i})$, $\sin\theta' \cos\phi'$ can be expressed as the function of θ and ϕ :

$$505 \quad \sin\theta' \cos\phi' = A_{11}\sin\theta\cos\phi + A_{12}\sin\theta\sin\phi + A_{13}\cos\theta \quad (\text{A3.3})$$

A_{ij} are represent the elements in matrix $A_R(\psi_x^{X,i}, \psi_y^{Y,i}, \psi_z^{Z,i})$ for $i, j = 1, 2, 3$.

Using (A3.2) and (A3.3), $\delta(\cos\alpha)$ can be expressed as a function of $\delta\theta$ and $\delta\phi$ as:

$$\delta(\cos\alpha) = (A_{11}\cos\theta\cos\phi + A_{12}\cos\theta\sin\phi - A_{13}\sin\theta)\delta\theta + (-A_{11}\sin\theta\sin\phi + A_{12}\sin\theta\cos\phi)\delta\phi \quad (\text{A3.4})$$

510 Finally, δR_s can be expressed as the function of δR , $\delta\theta$, $\delta\phi$ as:

$$\delta R_s = F(\delta R, \delta \theta, \delta \phi) = f_R(\theta, \phi)\delta R + f_\theta(\theta, \phi)\delta \theta + f_\phi(\theta, \phi)\delta \phi$$

$$(A3.5)$$

For:

$$f_R(\theta, \phi) = \frac{d^2 + R^2 - 2Rd(A_{11}\sin\theta\cos\phi + A_{12}\sin\theta\sin\phi + A_{13}\cos\theta)}{2[R - d(A_{11}\sin\theta\cos\phi + A_{12}\sin\theta\sin\phi + A_{13}\cos\theta)]^2}$$

$$515 \quad (A3.6)$$

$$f_\theta(\theta, \phi) = \frac{d(R^2 - d^2)(A_{11}\cos\theta\cos\phi + A_{12}\cos\theta\sin\phi - A_{13}\sin\theta)}{2[R - d(A_{11}\sin\theta\cos\phi + A_{12}\sin\theta\sin\phi + A_{13}\cos\theta)]^2}$$

$$(A3.7)$$

$$f_\phi(\theta, \phi) = \frac{d(R^2 - d^2)(-A_{11}\sin\theta\sin\phi + A_{12}\sin\theta\cos\phi)}{2[R - d(A_{11}\sin\theta\cos\phi + A_{12}\sin\theta\sin\phi + A_{13}\cos\theta)]^2}$$

$$(A3.8)$$

520 A.4 True error of E_2

See figure 4 (b); the total length of side AC and side AB represents the pulse width. Side AC equals side CB and they are both equal to half of the pulse width. In $X_i Y_i Z_i$, the presentation of point A is (x_i, y_i, z_i) , the receiver is $(0,0,0)$ and T_i is $(d,0,0)$. The distance between T_i and A is $R_i = R - R_s$. We denote that the presentation of point B and C in $X_i Y_i Z_i$ is (x_B, y_B, z_B) and (x_C, y_C, z_C) , respectively. We use vector collinear to establish equations for B and C. Therefore, one can

525 obtain the coordinates of point B and C by the following equations:

$$(x_B, y_B, z_B)^T = \frac{R_s - S}{R_s} (x_i, y_i, z_i)^T \quad (A4.1)$$

$$(x_C - d, y_C, z_C)^T = \frac{R_i - S}{R_i} (x_i - d, y_i, z_i)^T \quad (A4.2)$$

$$(x_i - d, y_i, z_i)^T \quad (A4.2)$$

For isosceles triangle ABC, the perpendicular line AD intersects side CB in middle point at the midpoint D. Then, we obtain

530 the coordinate value of D in $X_i Y_i Z_i$ as:

$$(x_D, y_D, z_D) = \frac{1}{2}(x_B + x_C, y_B + y_C, z_B + z_C) = \frac{1}{2}((a_1 + a_2)x_i - a_2d + d, (a_1 + a_2)y_i, (a_1 + a_2)z_i) \quad (A4.3)$$

We denote $a_1 = \frac{R_s - S}{R_s}$, $a_2 = \frac{R_i - S}{R_i}$. Finally, one can obtain the error vector of E_2 as vector \overrightarrow{DA} in $X_i Y_i Z_i$:

$$\overrightarrow{DA} = \left(\frac{(2 - a_1 - a_2)x_i + d(a_2 - 1)}{2}, \frac{2 - a_1 - a_2}{2} y_i, \frac{2 - a_1 - a_2}{2} z_i \right)^T \quad (A4.4)$$

535 **A.5 ~~calculate AoAs~~ Calculate AoA and range information in $X_i Y_i Z_i$**

For a space point (x_i, y_i, z_i) in $X_i Y_i Z_i$ which ~~represent~~ represents a MTSP, R_s can be solved easily as:

$$\begin{aligned} \vec{R}_s &= (x_i, y_i, z_i) \\ R_s &= \sqrt{x_i^2 + y_i^2 + z_i^2} \end{aligned} \quad (\text{A6.1})$$

The distance between transmitter T_i and receiver R_x is d_i as ~~sketched~~ shown in figure 4(a). Thus, the coordinate value of
540 T_i in $X_i Y_i Z_i$ is $(d_i, 0, 0)$ and R_i can be solved as:

$$R_i = \sqrt{(x_i - d_i)^2 + y_i^2 + z_i^2} \quad (\text{A6.2})$$

Before we calculate the AoAs in $X_i Y_i Z_i$, the representation of unit vectors of axis-X, Y, Z in $X_i Y_i Z_i$ ~~need~~ needs to ~~know~~ be known. In XYZ those unit vectors are easily represented as $(1,0,0)^T$, $(0,1,0)^T$, $(0,0,1)^T$. Though ~~coordinates~~ the coordinate rotation matrix $A_R(\psi_x^{X,i}, \psi_y^{Y,i}, \psi_z^{Z,i})$, one can get those unit vector's representation in $X_i Y_i Z_i$ as:

$$\begin{aligned} 545 \quad \vec{n}_x &= (A_{11}, A_{21}, A_{31})^T \\ \vec{n}_y &= (A_{12}, A_{22}, A_{32})^T \\ \vec{n}_z &= (A_{13}, A_{23}, A_{33})^T \end{aligned} \quad (\text{A6.3})$$

~~For~~ \vec{n}_x , \vec{n}_y and \vec{n}_z are unit vectors of Axis-X, Y, Z respectively. ~~And, and~~ A_{ij} are the elements ~~in~~ a 3×3 matrix $A_R(\psi_x^{X,i}, \psi_y^{Y,i}, \psi_z^{Z,i})$ for $i, j = 1, 2, 3$. Now ~~AoA~~ the AoA can ~~get~~ be obtained as:

$$550 \quad \cos \theta = \frac{\vec{R}_s \cdot \vec{n}_z}{R_s} \quad (\text{A6.4})$$

$$\sin \theta = \sqrt{1 - \cos^2 \theta} \quad (\text{A6.5})$$

$$\cos \phi = \frac{\vec{R}_s \cdot \vec{n}_x}{R_s \cdot \sin \theta} \quad (\text{A6.6})$$

$$555 \quad \sin \phi = \frac{\vec{R}_s \cdot \vec{n}_y}{R_s \cdot \sin \theta} \quad (\text{A6.7})$$

For $0^\circ < \theta < 180^\circ$ and $0^\circ \leq \phi < 360^\circ$. When $\theta = 0^\circ$, we handle it as same as in **Appendix (A.2)**.

560

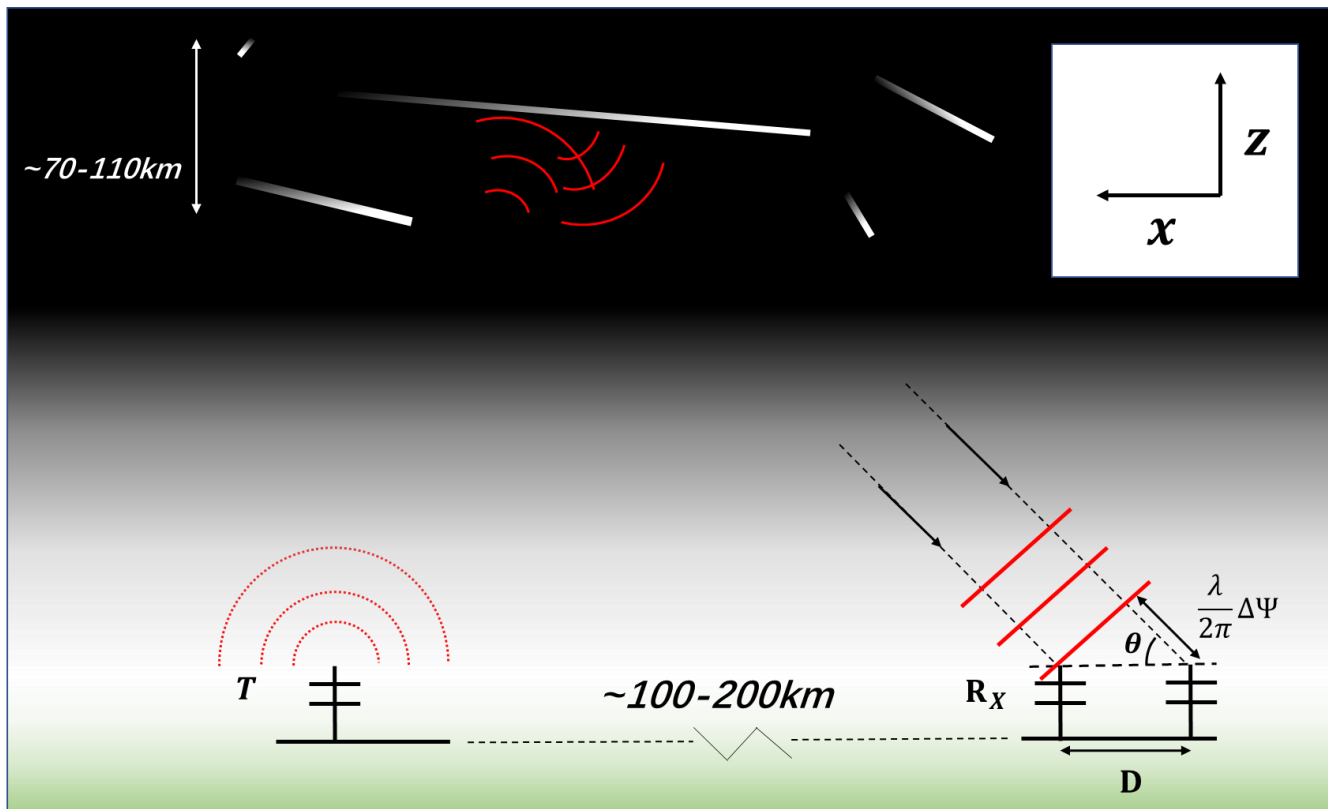


Figure 1: Schematic diagram of ~~a~~the simplified bistatic configuration used in Hocking's vertical resolution analysis (Hocking, 2018). The two ~~receiver~~receiving antennas and ~~a transmitter~~the transmitting antenna are collinear. The analysis is in a 2-dimensional vertical section through the baseline— ~~joining the antennas~~. The radio wave is scattered ~~by~~from a few Fresnel zones of several kilometres ~~long~~' length around ~~the~~ specular point ~~in~~on the meteor trail and received by ~~receiver~~the receiving antennas. The cross-correlation analysis between ~~receiver~~the receiving antennas can ~~be used to solve for~~ the AoAs. ~~The fact that~~Because the radio wave ~~bounced back~~is reflected from a ~~region a~~ few Fennel zones ~~will cause~~in length the measured phase difference between the receiver antenna ~~pair~~ ~~deviating~~pairs to deviates from the ideal phase difference. ~~The ideal phase difference will solve an~~ AoAs pointing to ~~MTSP~~. This deviation from the ideal phase difference is one of the error sources ~~of~~in the PDME. ~~In this work, we solve for the ideal phase difference associated with the AoA directed to the MTSP.~~

565

570

575

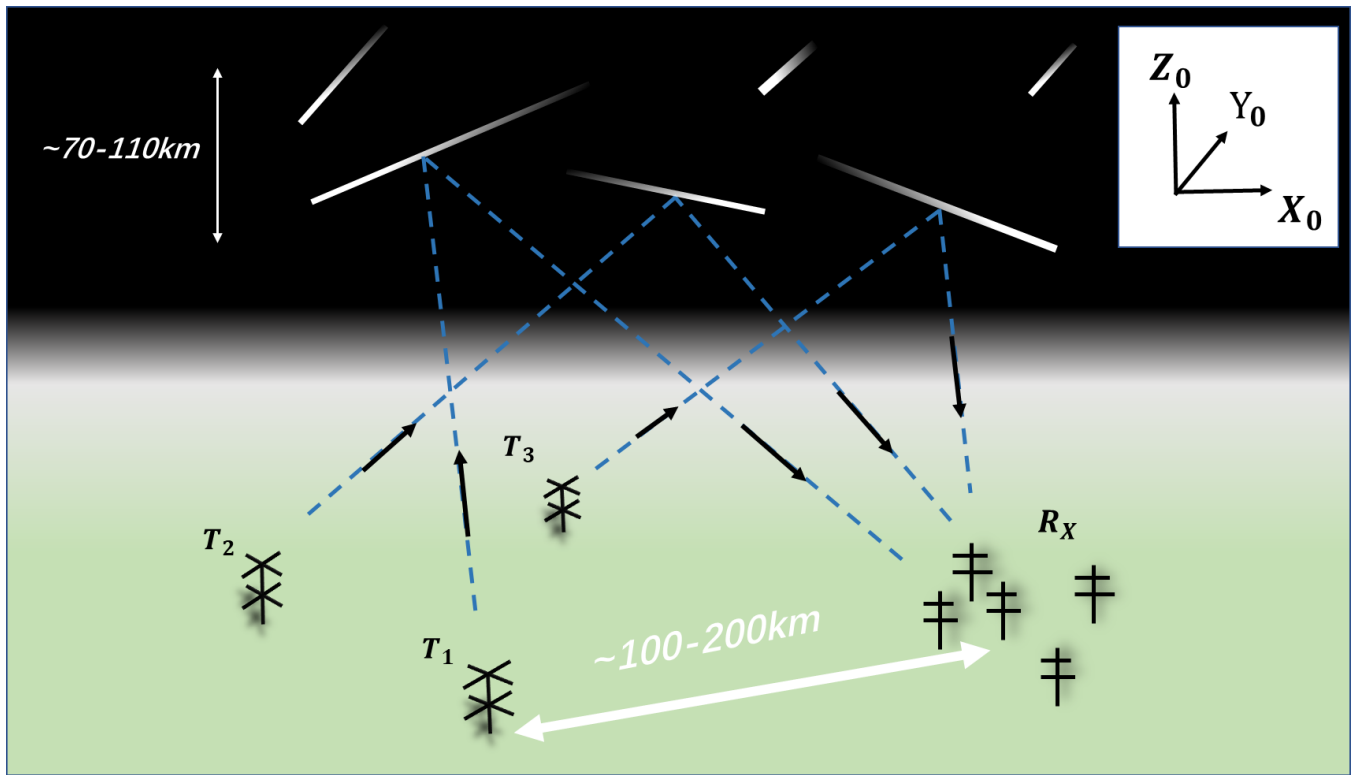


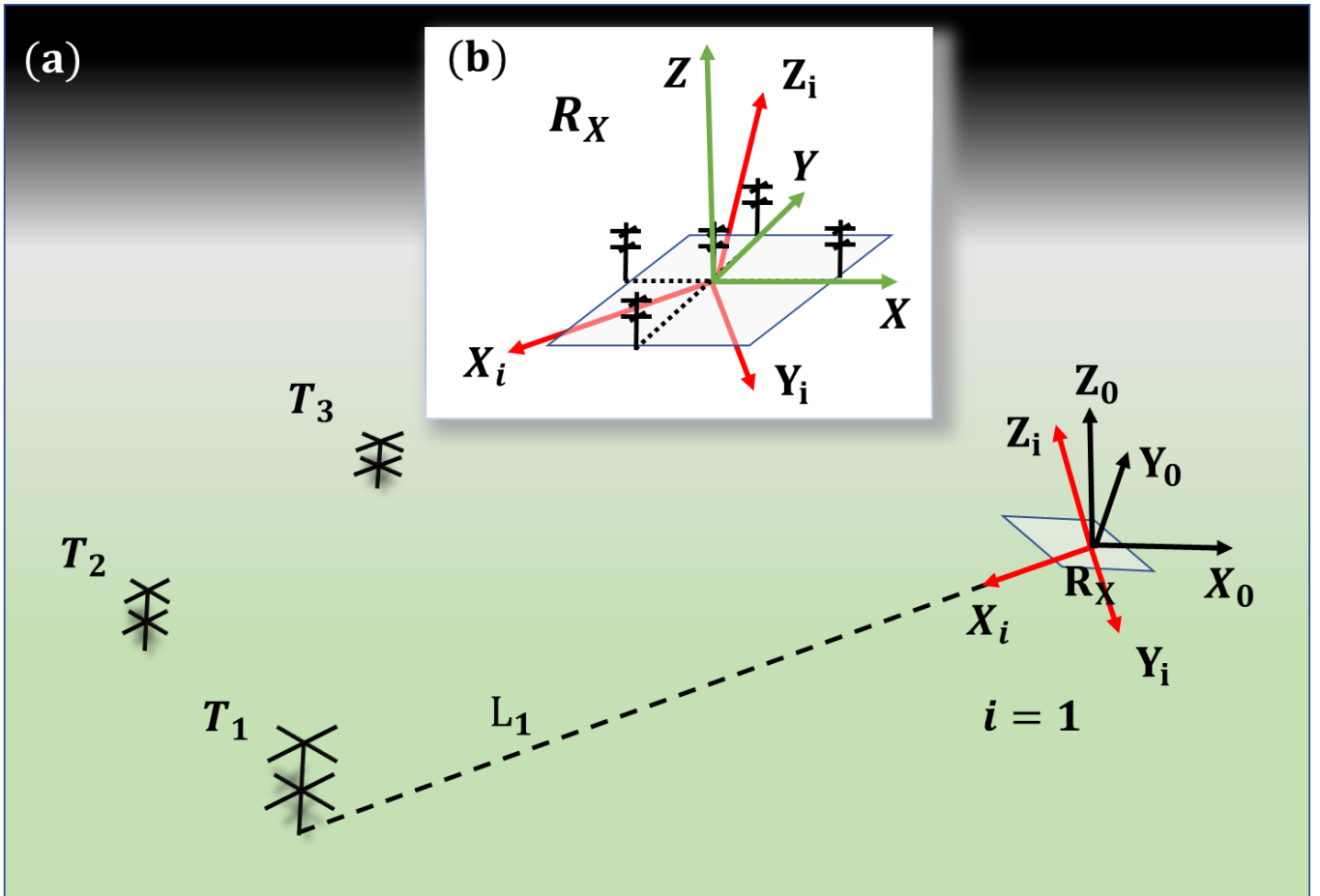
Figure 2: Schematic diagram of a multistatic meteor radar system using SIMO (single-input and multi-output). There are three transmitters (T_1, T_2 and T_3) and one receiver (R_X) in the picture. The transmitter/receiver distance is **usually approximately typically** 100-200 km. X_0, Y_0, Z_0 represents the east, north and up directions of the **receiver-receiving antenna**. Over 90% of the received energy comes from about one kilometre around **the** specular point of the meteor trail, which is slightly less than the length of the central Fresnel zone (Ceplecha et al., 1998).

580

585

590

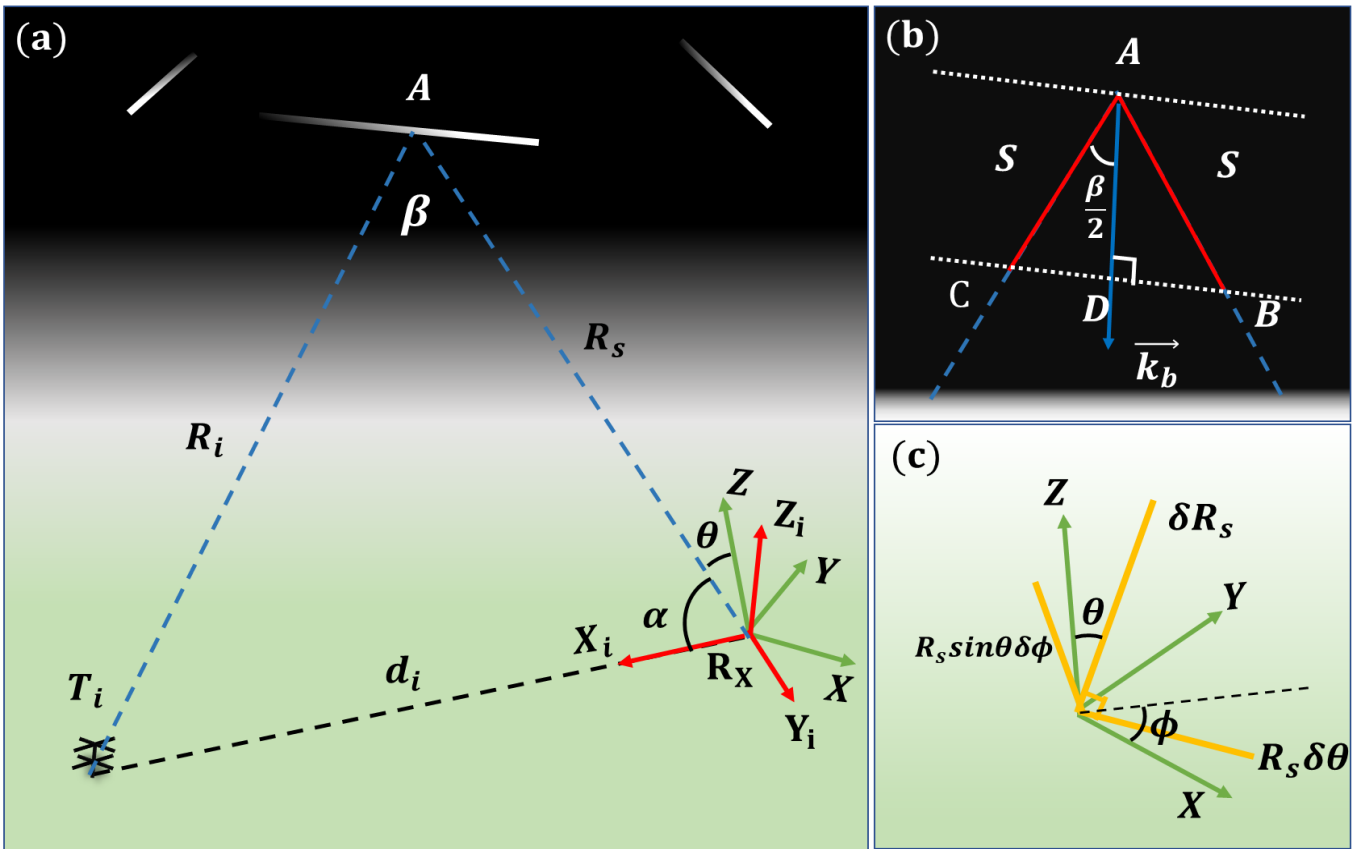
595



600 Figure 3: (a) Schematic diagram of the three ~~introduced~~ coordinate systems used in this work. $X_i Y_i Z_i$ are a class of coordinate systems whose axis- X_i pointpoints to transmitter I, with, i. ~~And in this picture, i are $\equiv 1,2,3$.~~ $X_0 Y_0 Z_0$ is the ENU coordinate system and to which all errors will beare compared in this coordinate. (b) Magnified plot of the ~~receiver-receiving~~ array. XYZ is fixed on the receiver horizontal plane. Axis- X and Y are collinear ~~to~~ with the two arms of the antenna ~~arrays~~ array.

605

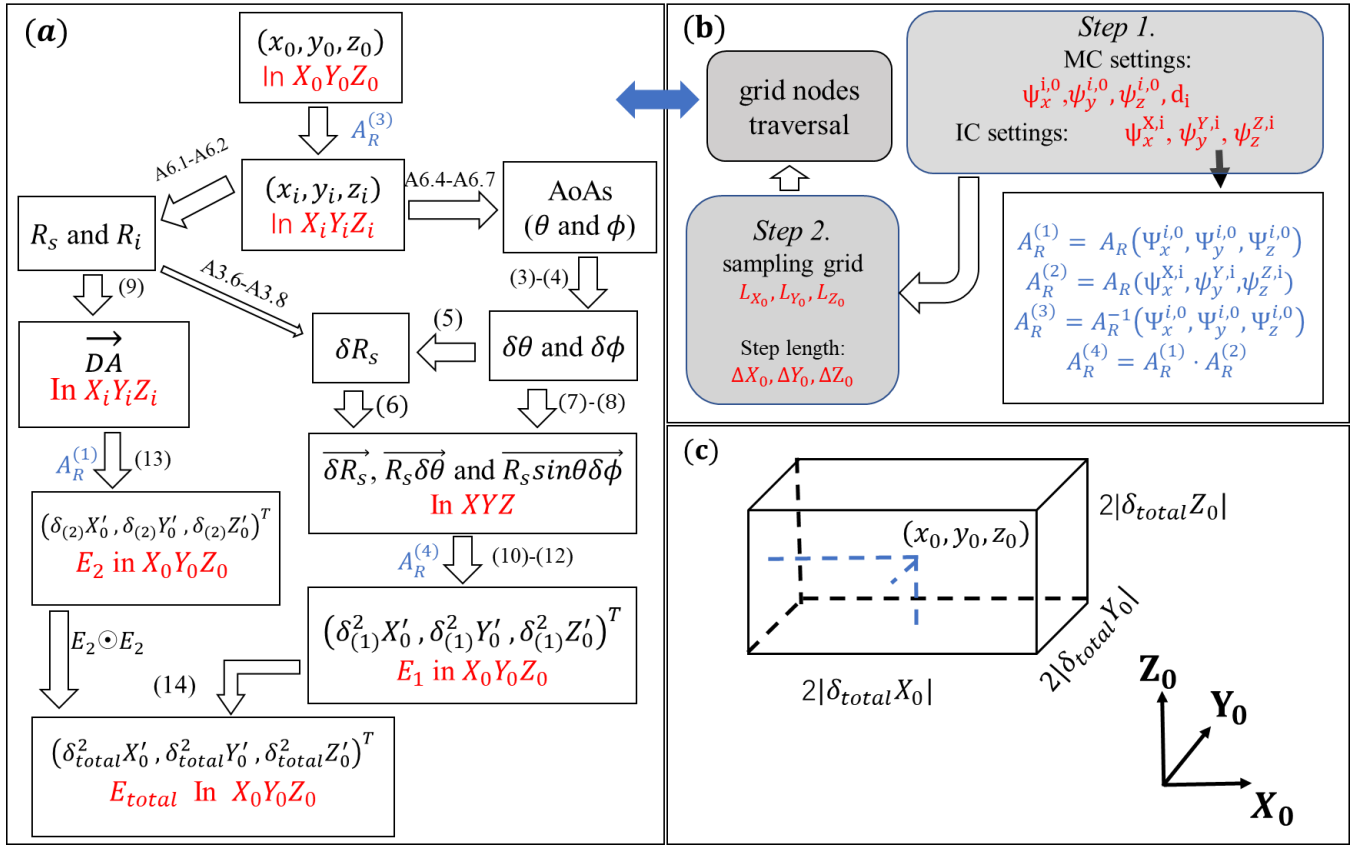
610



615 Figure 4: (a) Schematic diagram of the forward scatter geometry for the radar link between T_i and R_x . Point-A is the MTSP. (b) Magnified plot of specular point A. The red line represents a radio wave pulse, and S is the half wave-pulse length. \vec{k}_b is the Bragg vector which halves the forward scatter angle β . (c) Schematic diagram of E_1 in XYZ, which can be decomposed into three orthogonal vectors.

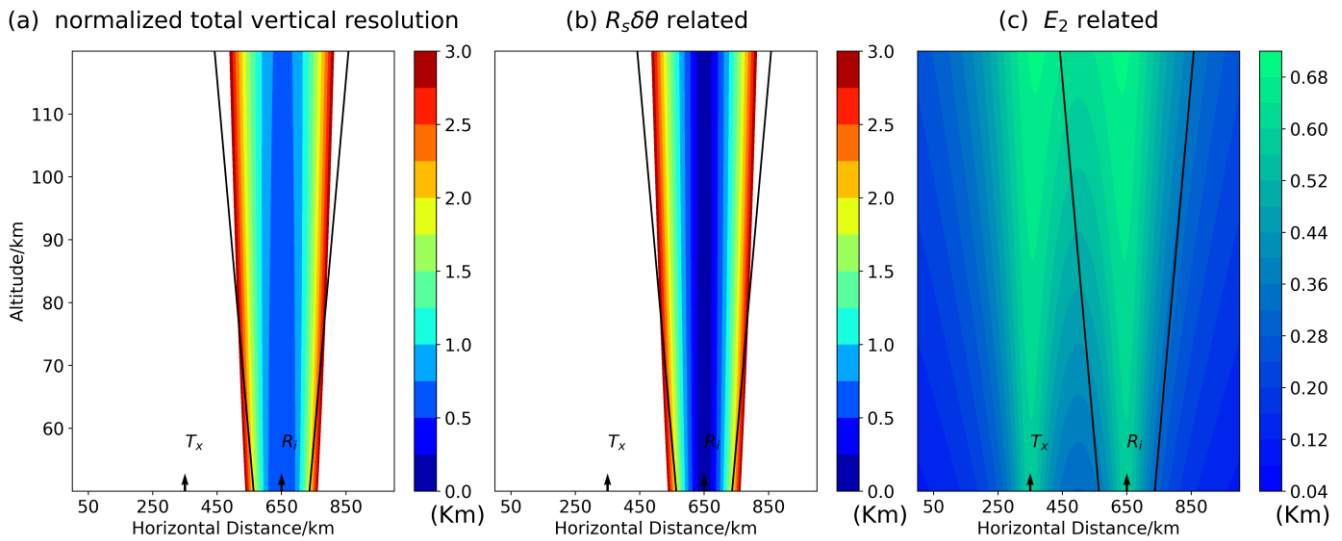
620

625



630 Figure 5: (a) the flow chart of the location error calculation process for a point in $X_0Y_0Z_0$. The marknotation beside arrows represent the corresponding equations (black) or coordinate rotation matrix (blue) in the paper. “ \odot ” is the Hadamard product. Thus $E_2 \odot E_2$ will getyield $(\delta_{(2)}^2 X_0, \delta_{(2)}^2 Y_0, \delta_{(2)}^2 Z_0)^T$. (b) the flow chart of the program to calculate the location errors distributions for a radar link L_i . This process includes parameters settings for a radar link, generating; the generation of the sampling grid nodes and the traversing of all the nodes. For each node, the program uses the calculation method described in (a). MC: is the multistatic configuration, IC: is the interferometer (receiver antennasreceiving antenna) configuration. (c) Schematic diagram of the relationship between the spatial resolution and the total location errors of the MTSP. For a detected point in space, the MSE of MTSP's location errors is $\pm|\delta_{total}X_0|$, $\pm|\delta_{total}Y_0|$, $\pm|\delta_{total}Z_0|$ in the zonal, meridian/meridional and vertical directions, respectively. This means that the actual specular point might occur in a region which formforms a $2|\delta_{total}X_0| \times 2|\delta_{total}Y_0| \times 2|\delta_{total}Z_0|$ cube and the detected point is on the centralcentroid of this cube.

635



645

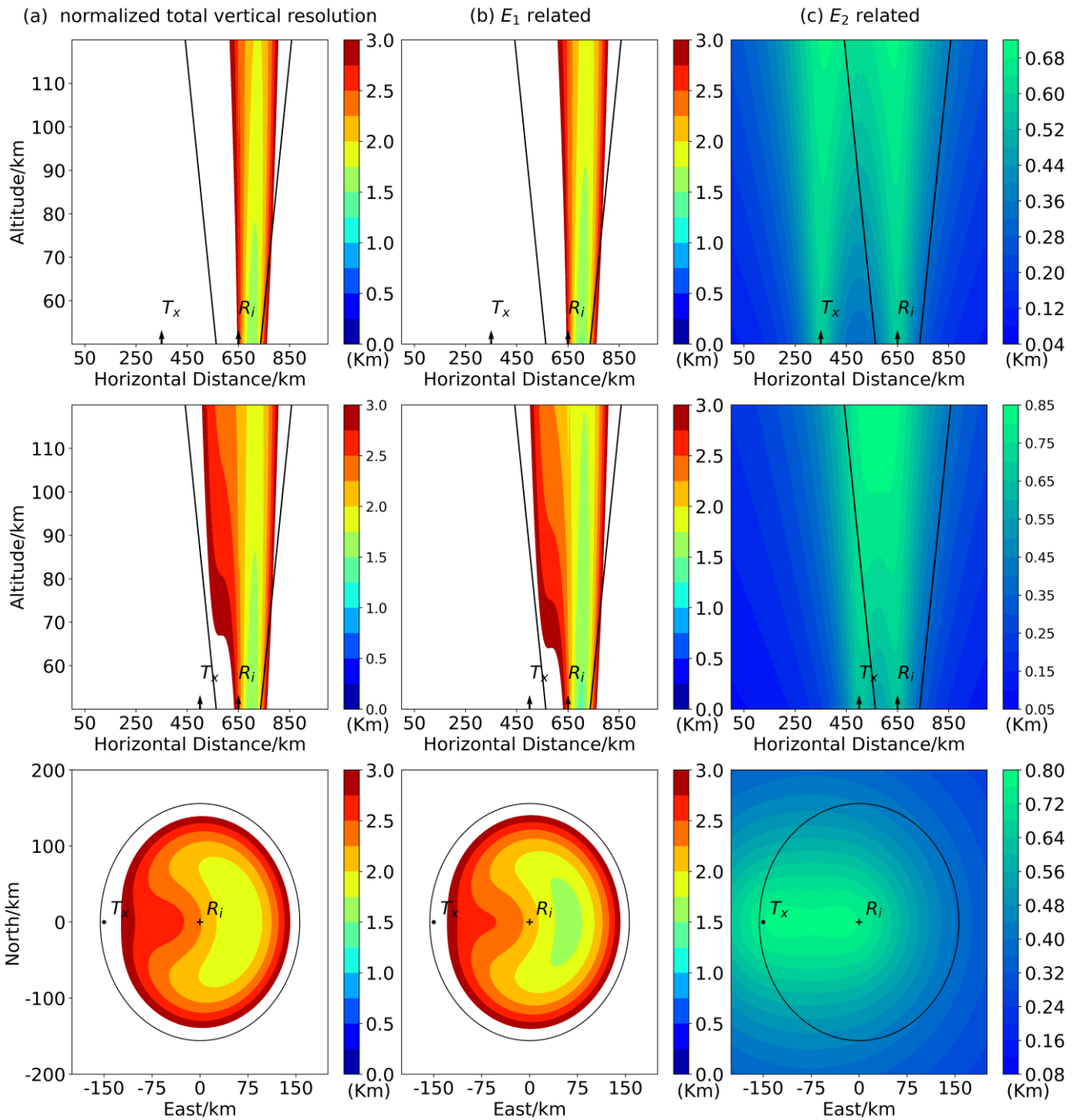
Figure 6: the normalized vertical resolution distribution in a vertical section from 50 km to 120 km height when ~~ignore~~ the error term " δR_s " ~~is ignored~~. Panels (a), (b), and (c) are the total, $R_s \delta \theta$ related, and E_2 related normalized resolution ~~distribution~~ ~~distributions~~, respectively. ~~The~~ ~~These~~ results ~~is~~ ~~these~~ ~~are~~ ~~the~~ ~~same~~ ~~as~~ ~~those~~ ~~produced~~ ~~in~~ Hocking's work (Hocking, 2018). ~~Two~~ ~~The~~ ~~two~~ black arrows represent the positions right above the transmitter (Tx) and the receiver (Rx) and the transmitter/receiver ~~are~~ ~~separation~~ ~~is~~ ~~300~~ ~~km~~ ~~away~~. The region between the two black oblique lines is ~~a~~ ~~the~~ ~~trustworthy~~ ~~sampling~~ ~~volume~~ for the ~~receiver~~ ~~receiving~~ ~~array~~ because the elevation angle is beyond 30° ~~with~~ ~~little~~ ~~to~~ ~~reduce~~ influence ~~of~~ ~~from~~ potential mutual antenna coupling or ~~from~~ other obstacles in the surrounding ~~area~~. Except the region ~~in~~ ~~at~~ large elevation ~~angle~~ ~~angles~~ (i.e., 90°), the E_2 related resolution values are much lower than the $R_s \delta \theta$ related ~~errors~~. The $R_s \delta \theta$ related resolution distribution ~~is~~ ~~depends~~ only ~~depend~~ on the ~~receiver~~ ~~receiving~~ ~~antennas~~. Thus, the total vertical resolution distribution is nearly unchanged with the variation of the transmitter/receiver distance ~~varying~~. ~~The~~ ~~normalized~~ ~~Normalized~~ resolution values ~~that~~ exceed 3 km (which correspond 12 km vertical resolution ~~area~~ ~~are~~ ~~not~~ shown).

650

655

660

665



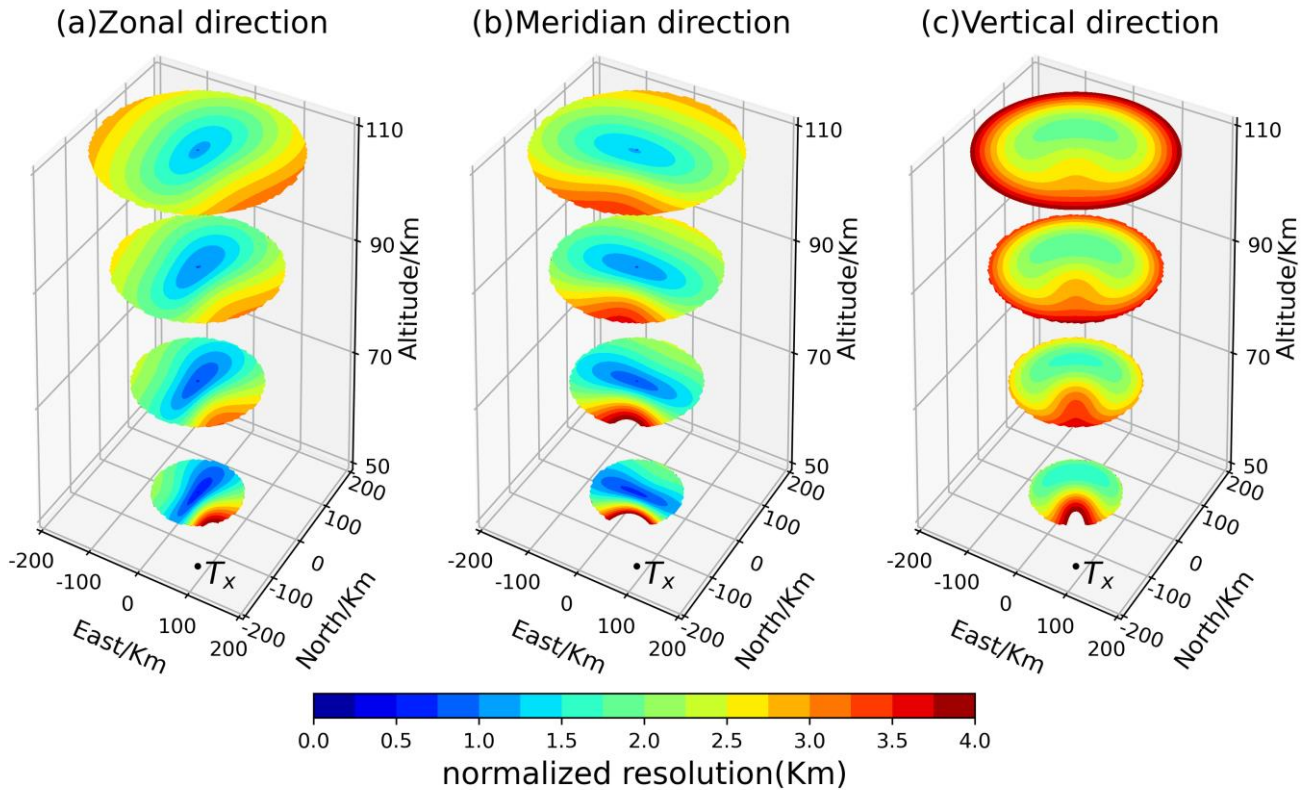
670

Figure 7: the normalized vertical resolution distribution using the analytical method described in this paper. The first and second rows represent a vertical section from of height from 50 km to 120 km. The third row represent represents the horizontal section in at 90 km and the receiver receiving array is on at the origin with positive coordinate value represent east values representing the eastward or north direction northward directions, respectively. The first row has the same parameters settings as Figure 6 and is used to compare with Figure 6. The E_1 related resolution will change with the transmitter/receiver configuration because it

675

~~consider~~considers the error term “ δR_s ”. Thus, the total vertical resolution will change with the transmitter/receiver configuration. With the transmitter/receiver distance varying from 300 km (the first row) to 150 km (the second row), the total vertical resolution distribution is clearly changed. The third row is the perspective to the horizontal section inat 90 km altitude for the second row. The ~~normalized~~Normalized resolution values that exceed 3 km ~~aren~~are not shown.

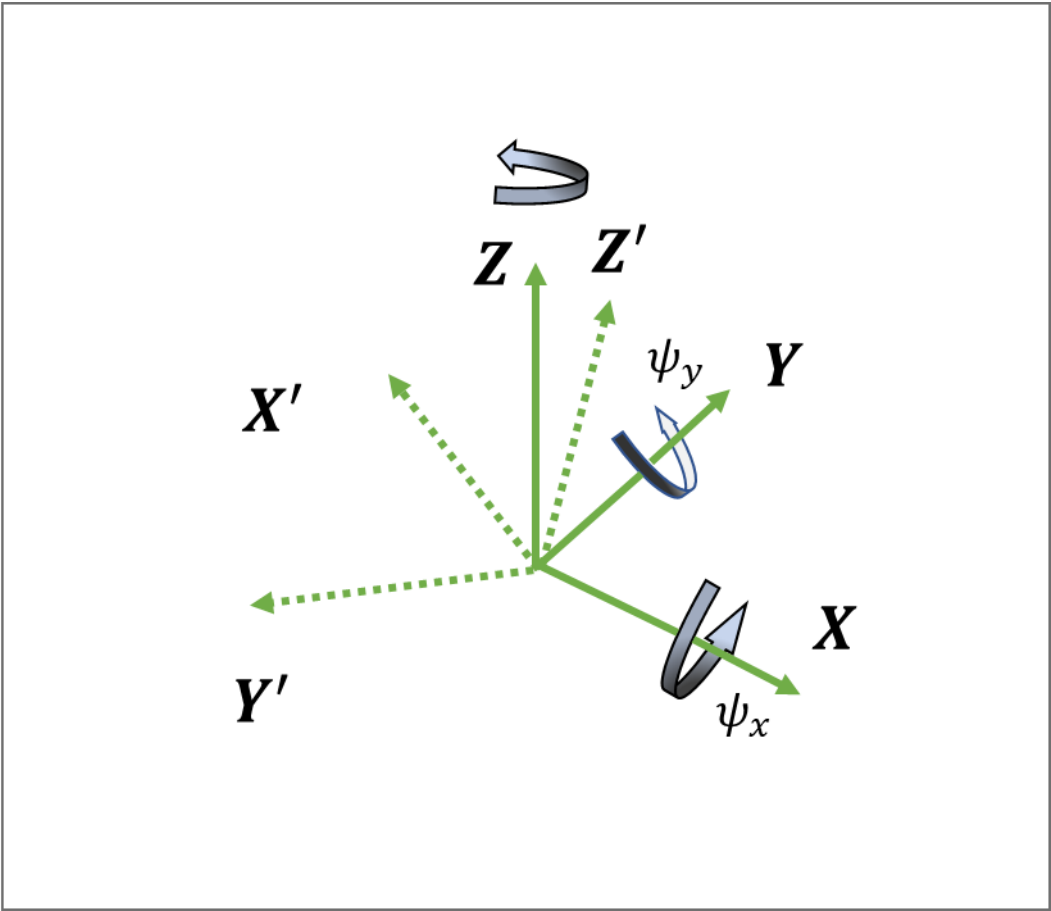
680



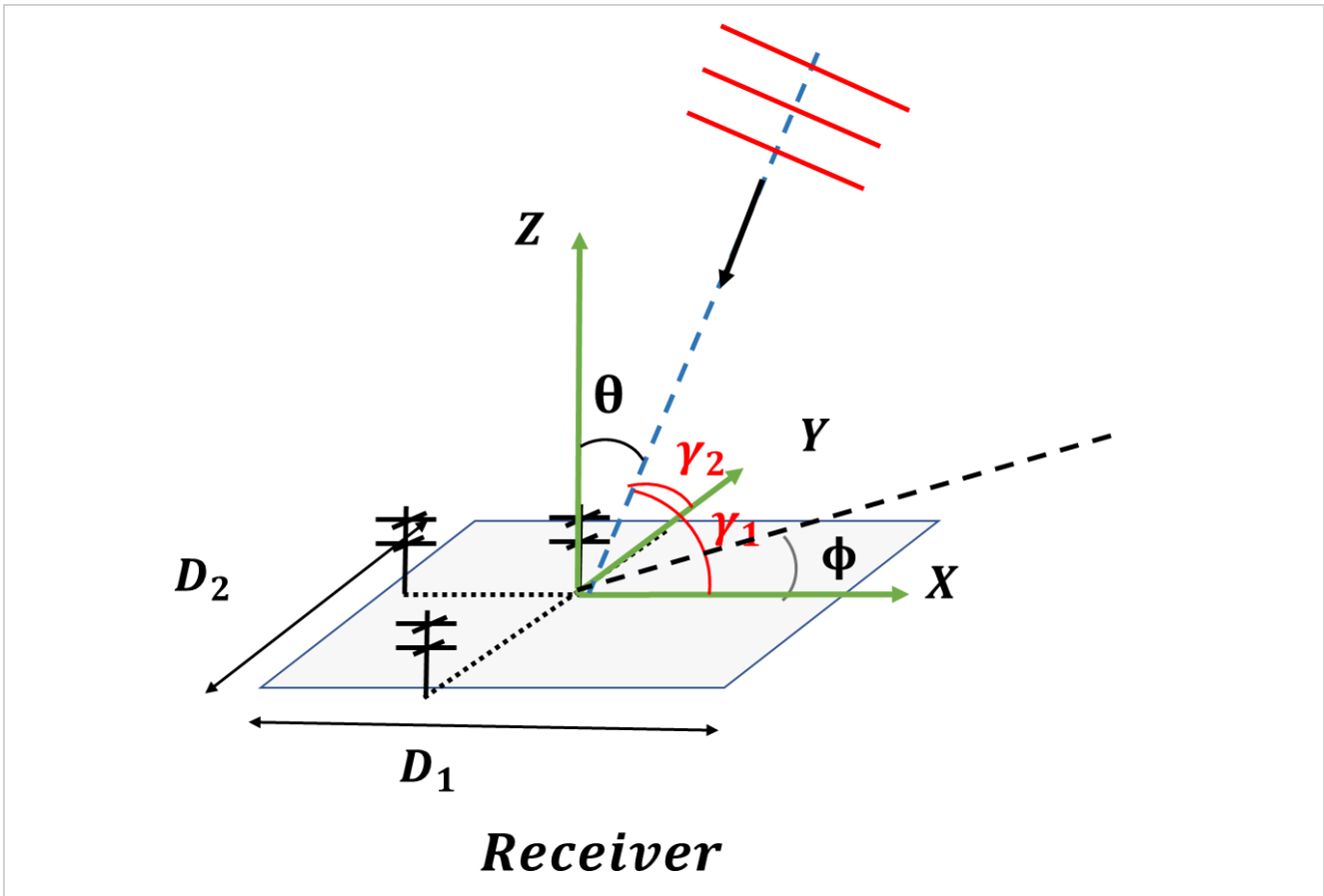
685

Figure 8: ~~the 3D contour~~contour plot of the normalized resolution distribution for a multistatic radar link whose baseline length is 180 km and whose transmitter is south by east 30° of the receiver. The black dots represent the position right above the transmitter and the ~~receiver~~receiving array is onat the origin of the axes. (a), (b) and (c) are the normalized resolution distributionsdistributions in the zonal, ~~meridian~~meridional and vertical directions, respectively. The subplot's four slice ~~circles~~circles from bottom to top are the horizontal section in 50 km, 70 km, 90 km and 110 km height, respectively. The region whose elevation angle of the receiver is less than 30° ~~isn~~is not shown and therefore the slice circles become larger from the bottom to the top. The ~~normalized~~Normalized resolution values that exceed 4 km (which ~~correspond~~corresponds to 16 km resolution ~~aren~~are not shown).

690



695 Figure A.1



700 Figure A.2 ~~(two~~ The receiving array geometry (only three antennas are not shown for conciseness)